AD-A065 366 AIR FORCE INST OF TECH WRIGHT-PATTERSON AFB OHIO F/G 3/2
CORONAL STRUCTURE AND PROMINENCE CHARACTERISTICS RELATIVE TO IN--ETC(U)
JUL 78 J F BRYSON

UNCLASSIFIED AFIT-CI-79-75T NL

1 OF 1
ADA
065366

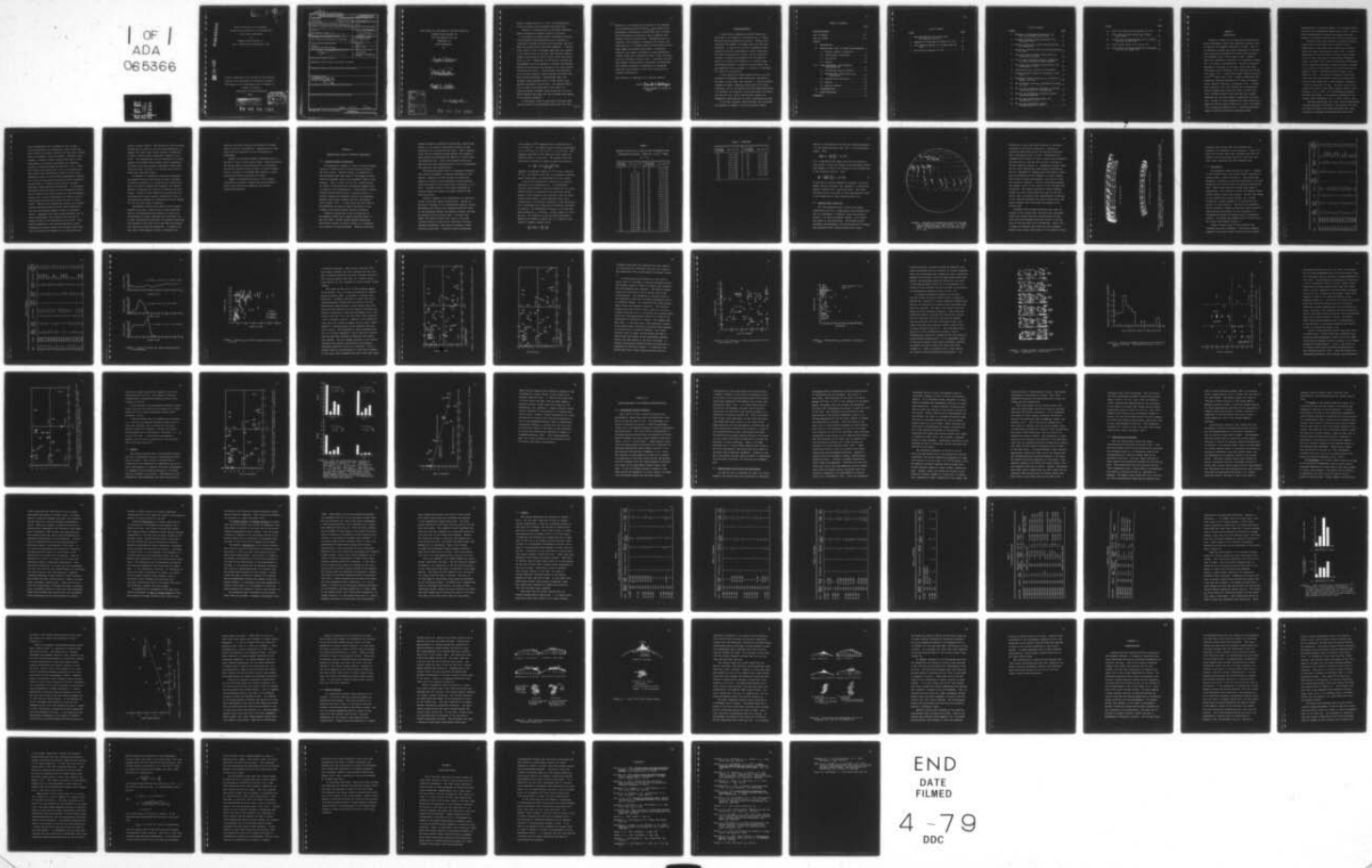

END
DATE
FILMED
4-79
DDC

Coronal Structure and Prominence Characteristics Relative to Instabilities in the Solar Atmosphere

by

Joseph Francis Bryson, Jr.

B.S., University of Washington, 1970

A thesis submitted to the Faculty of the Graduate School of the University of Colorado in partial fulfillment of the requirements for the degree of Master of Science

Department of Astro-Geophysics

1978

UNCLASSIFIED

SECURITY CLASSIFICATION OF THIS PAGE (When Data Entered)

REPORT DOCUMENTATION PAGE	READ INSTRUCTIONS BEFORE COMPLETING FORM
1. REPORT NUMBER CI-79-75T	2. GOVT ACCESSION NO. (9) Master's thesis.	3. RECIPIENT'S CATALOG NUMBER
4. TITLE (and Subtitle) (6) Coronal Structure and Prominence Characteristics Relative to Instabilities in the Solar Atmosphere	5. TYPE OF REPORT & PERIOD COVERED Thesis
	6. PERFORMING ORG. REPORT NUMBER
7. AUTHOR(s) Capt Joseph F. Bryson, Jr. (10) Joseph Francis/ Bryson, Jr	8. CONTRACT OR GRANT NUMBER(s) (12) 91 p.
9. PERFORMING ORGANIZATION NAME AND ADDRESS AFIT student at the University of Washington	10. PROGRAM ELEMENT, PROJECT, TASK AREA & WORK UNIT NUMBERS (11) 21 Jul 78
11. CONTROLLING OFFICE NAME AND ADDRESS AFIT/CI Wright-Patterson AFB OH 45433	12. REPORT DATE 1978 13. NUMBER OF PAGES 80
14. MONITORING AGENCY NAME & ADDRESS(if different from Controlling Office) (14) AFIT-CI-79-75T	15. SECURITY CLASS. (of this report) UNCLASSIFIED 15a. DECLASSIFICATION/DOWNGRADING SCHEDULE

16. DISTRIBUTION STATEMENT (of this Report)

Approved for public release, distribution unlimited

17. DISTRIBUTION STATEMENT (of the abstract entered in Block 20, if different from Report)

18. SUPPLEMENTARY NOTES

JOSEPH P. HIPPS, Major, USAF
Director of Information, AFIT

FEB 8 1979

19. KEY WORDS (Continue on reverse side if necessary and identify by block number)

20. ABSTRACT (Continue on reverse side if necessary and identify by block number)

012 200

DD FORM 1 JAN 73 1473 EDITION OF 1 NOV 65 IS OBSOLETE

UNCLASSIFIED

SECURITY CLASSIFICATION OF THIS PAGE (When Data Entered)

This thesis for the Master of Science Degree by

Joseph Francis Bryson, Jr.

has been approved for the

Department of

Astro-Geophysics

by

Donald E. Billings

Donald E. Billings

J. McKim Malville

J. McKim Malville

Dwight R. Nicholson

Dwight R. Nicholson

Date 21 July 1978

Bryson, Joseph Francis, Jr. (M.S., Astro-Geophysics)
Coronal Structure and Prominence Characteristics
Relative to Instabilities in the Solar Atmosphere
Thesis directed by Professor Donald E. Billings

An analysis of λ5303 coronal filtergrams obtained from Sacramento Peak Observatory and an analysis of prominence lifetimes obtained from Fraunhofer Institute Maps and H-alpha patrol film were completed. A statistical survey of the filtergrams shows that the presence of the λ5303 corona on the east limb indicates chromospheric Active Regions (AR's) coming within the earth's field of view. Comparison of the coronal features and chromospheric activity suggests a possible relationship between the definition and heights of the λ5303 coronal structures and flares. Configurations and definition of the coronal magnetic fields inferred from λ5303 and Mount Wilson photospheric magnetograms imply that stressed fields possibly exist in some coronal loop systems associated with the AR's. The sharper definition of some of the loops may be the result of a current-produced azimuthal field around the flux tube which confines the plasma and thus increases the density of the emitting material.

A statistical study of prominence lifetimes shows that the ratio of the prominence angle from the local

next page

cont. meridian to its length may be related to the lifetime of the prominence before eruption. This implies that photospheric differential rotation may induce currents into prominences by stretching their footpoints and, thereby, produce instabilities. Prominences that are located in the proximity of emerging flux regions and those that are in filament cavities which border coronal holes appear less stable than others. Prominence stability also seems to decrease in those prominences located along young, developing neutral lines and along very old, declining neutral lines. A possible relationship between flare-producing mechanisms and mechanisms that produce eruptives in prominences is suggested based upon the analysis of the λ5303 corona and the filament observations.

This abstract is approved as to form and content.

Signed Donald E. Billings

Faculty member in charge of thesis.

ACKNOWLEDGEMENTS

I would like to express my genuine thanks and gratitude to Dr. Donald E. Billings and Dr. J. McKim Malville who have guided this project. Without their assistance and wisdom, this paper would not have been completed. It was at Dr. Billing's suggestion that I studied the Fe XIV, monochromatic survey filtergrams for their relationship to flares, and Dr. Malville's interest in eruptive prominences that initiated my search for current flow predictors in coronal loops. I am extremely grateful to them for sharing their time and experience with a newcomer struggling to understand the field of solar physics.

I also express my sincere appreciation to all the personnel at Sacramento Peak Observatory, New Mexico, who made my visit there very pleasant. I am particularly indebted to Howard DeMastus and Don Neidig for their assistance, and to the Neidigs for their warm hospitality. I am grateful to my sponsor, the United States Air Force, who paid the bill, and to the National Oceanic and Atmospheric Administration for their assistance and data.

To my wife, Boonyuen, whose patience and understanding exceeds all bounds, I give the greatest thanks.

TABLE OF CONTENTS

LIST OF TABLES

LIST OF FIGURES

FIGURE PAGE

CHAPTER I

INTRODUCTION

Studies of flares and of eruptive prominences have seldom overlapped, except when eruptives occurred within the spatial and temporal proximity of flares. Then it is generally accepted that major disruptions in the magnetic fields which produced the flares also disrupted the filaments (Rust, 1976; Priest, 1976). However, flares are essentially explosions in a magnetized plasma and, in a sense, so are eruptives. Flares are generally believed to originate in the lower corona just where prominences occur (Sturrock, 1972; Heyvaerts and Priest, 1977; Rust, 1977). Flares have energy outputs typically of 10^{30-32} ergs (Rust, 1977); eruptive prominences have comparable energies approaching 10^{31} ergs of released energy (Engvold, Malville, and Rustad, 1976). Furthermore, Sturrock (1967) has proposed that reconnections within filaments may change the shear in field lines into a twisted filament which may then be a storage mechanism for the flare energy released upon its eruption. Fields in active filaments are often twisted and appear to untwist before flares occur (Zirin and Tanaka, 1973; Jockers and Engvold, 1975). Pre-flare filaments appear to deviate greatly from potential field

configurations in that they appear to be stressed fields which may store substantial energy (Rust, 1977). Most of these observations of filament activations have been studied in connection with pre-flare build-up activities.

Generally, the flare theories are based on several models which include some form of magnetic field annihilation in the lower corona resulting in current sheets and rapid Joule heating (Rust, 1976). Popular mechanisms for the production of flares involve emerging flux tubes resulting in reconnections (Heyvaerts, Priest, and Rust, 1976), shear from twisted photospheric fields caused by penumbral convection around a sunspot or by rotation of the sunspot, and relative motions of magnetic fields of opposite polarity (Tanaka, 1976; DeMastus, 1977). The energy is probably transmitted along the flux tubes through twisting or plasma waves into the lower corona and is then suddenly released as a flare at some point in time. This may occur within single flux tubes as some models suggest (Spicer, 1976; Petrasso, et al., 1976), or in reconnections between multiple flux tubes, as is generally accepted for the larger flares (Heyvaerts, et al., 1976a; Priest, 1976).

The basic mechanisms that cause eruptive prominences, including quiescent prominences, are probably the same as those for flares, and those mechanisms that cause eruptions of quiescent prominences may differ from

active prominences only in degree and not in type. Active prominences are footpointed in much higher magnetic fields with larger gradients and more rapid changes than are quiescents, and are probably, therefore, more unstable. However, dynamic changes also seem to occur continuously in quiescent prominences and apparent twisting is sometimes observed (Engvold, et al., 1976). The twisting and changes that occur in prominence elements imply that field-aligned currents flow in both quiescent as well as active region prominences, probably as a result of the relative motions of their footpoints, and may result in energy storage through increased azimuthal fields around the prominences. In quiescents, the relative motions could be from photospheric differential rotation and lateral motions of weak photospheric fields, and in active prominences the motions could be from sunspot rotations and lateral motions of strong fields. Emerging flux regions may disrupt this storage process through reconnections and field annihilation with the pre-existing magnetic fields of the prominences. Quiescents are longer-lived phenomena than are active prominences, which implies that the rate of energy storage in the quiescents may be slower. This might be expected if the driving mechanism is solar differential rotation rather than the more rapid rotations or motions with emerging flux regions that may

exist in active regions. Even though the rate of energy storage may be slower in the long-lived quiescents, it appears that their total energy release is comparable to that of active region prominences (Engvold, et al., 1976). This implies that critical currents or critical amounts of available stored energy must be comparable for both active and quiescent prominences before eruptives may occur, and that it is through their rate of energy gain that they differ.

In Chapter II lifetimes of quiescent prominences are measured and the relationship of these lifetimes to possible predictors of current-driven instabilities which may lead to "disparition brusques" are studied. Effects of emerging flux regions on eruptives are discussed. Chapter II also examines the possibility that over-burdening coronal magnetic fields play a role in the stabilizing process for prominences and that changes in this field may lead to eruptions.

The magnetic fields which overlie active regions probably also play a strong role in flare production. Much of the observations and studies of flares have concentrated in dynamic phenomena and transients; not as much literature has been seen on quiescent structures and features of the lower corona and their association with flares and eruptive prominences. In Chapter III the lower coronal magnetic fields, structures, and

features, and their possible relationship to chromospheric activity, are examined. Observations of λ5303 corona are also observed for any relationship to prominences.

Chapter IV discusses possible interpretations of the data in view of some current ideas. Some conclusions are reached about the characteristics of prominences and coronal characteristics relative to active regions. Current literature is reviewed that suggests a strong relationship between eruptions and flares.

Chapter V discusses the uses of λ5303 coronal filtergrams and further studies that may be needed to obtain flare prediction parameters and eruptive prominence predictors.

CHAPTER II

OBSERVATIONAL STUDY OF ERUPTIVE PROMINENCES

2.1 Possible Causes of Eruptives

As discussed in Chapter I, there are three probable causes of instabilities of current-carrying fields in the lower corona. Relative motions of footpoints in the photosphere may cause shear of the magnetic fields inducing increased currents and azimuthal fields in prominences. This, in turn, may act as a storage device for energy as the prominence increasingly departs from a potential field configuration. This process of energy storage should continue until a critical current is reached, whereby the azimuthal field of the prominence becomes sufficiently stronger than the longitudinal field (Parker, 1977). At this stage the flux tubes of the prominence may kink or buckle and result in the release of the stored energy through an eruptive.

Footpoint motions may be due to rotations of photospheric fields which induce torsional shears in the flux tubes, lateral motions between footpoints, which might stretch or distort fields, or to differential rotation of the photosphere. Relative velocities

between footpoints induced by differential rotation may create a $\underline{v} \times \underline{b}$ current which should increase as the footpoints are stretched further apart. Small reconnections from the shearing process between the arcades of loops across the prominence may result in a field along the prominence axis. This field-aligned current may then grow with the prominence moving into an increasingly non-potential field configuration.

This second probable cause of prominence instabilities should be emerging or changing photospheric flux regions. Emerging flux may disrupt the underlying supporting fields for the prominence through reconnections and magnetic field annihilation (Heyvaerts, et al., 1976). Adjacent flares or flare waves generated by distant flares also appear to produce unstable prominence structures.

Finally, changes in the configuration of overlying coronal fields may induce instabilities. Through reductions or changes in the overburdening magnetic fields, prominences may erupt if the unbalanced vertical force of the prominence exceeds the magnetic pressure that may be exerted by the overlying field. One might then expect that areas of open field lines or very weak overlying coronal fields may be associated with more unstable prominences, than those of stronger, closed overlying structures. A typical eruptive prominence

with a mass of 10^{15} grams may have an acceleration of 3×10^3 cm s^{-2}. The upward force is mass x acceleration, or $F \simeq 10^{15}$ gm x $(3 \times 10^3$ cm $s^{-2}) = 3 \times 10^{18}$ dyn. The downward force due to the overlying corona should be $(B^2/8\pi)A$ where A is the area. The average field that would have to contain an eruptive should be given by

$$B^2 = \frac{8\pi F}{A} = \frac{8\pi \times (3 \times 10^{18}) \text{ dyn}}{10^{19} \text{ cm}^2} ,$$

assuming a prominence length of 10^{10} cm and a width of 10^9 cm. The coronal field then is estimated as approximately three Gauss, not unreasonable for the corona.

The idea of differential rotation as an eruptive mechanism is an interesting one. If differential rotation could produce a current aligned with the longitudinal field of a prominence with continued current growth as the footpoints are stretched, then the large current could induce a large azimuthal field, kink instabilities, and eventual disruption of the prominence. For a prominence with footpoints at different latitudes (ϕ_1 and ϕ_2), the differential velocity, v_s of the endpoints would be $v_s = B\{\sin^2\phi_1 - \sin^2\phi_2\}$ where $B = 2.16^o$ per day. The values of v_s may be found from Table 1. Equating the change in energy due to a current to the change in magnetic energy yields

$$\frac{d}{dt}\left[\tfrac{1}{2}J^2 \mathcal{L} \ell\right] = \frac{B^2}{\mu_o} A \frac{d\ell}{dt} ,$$

TABLE 1

ABSOLUTE VELOCITY OF A POINT ON THE PHOTOSPHERE FROM DIFFERENTIAL ROTATION. BASED ON ($B \sin^2\theta$), WHERE $B = 2.16$

Latitude in Degrees	Vel (cm s^{-1})	Latitude in Degrees	Vel (cm s^{-1})
0	0	25	5.5×10^3
1	9.2	26	5.8×10^3
2	3.7×10^1	27	6.3×10^3
3	8.3×10^1	28	6.7×10^3
4	1.5×10^2	29	7.2×10^3
5	2.3×10^2	30	7.6×10^3
6	3.3×10^2	31	8.1×10^3
7	4.5×10^2	32	8.5×10^3
8	5.9×10^2	33	9.0×10^3
9	7.4×10^2	34	9.5×10^3
10	9.2×10^2	35	10.0×10^3
11	1.1×10^3	36	1.05×10^4
12	1.3×10^3	37	1.1×10^4
13	1.5×10^3	38	1.2×10^4
14	1.8×10^3	39	1.2×10^4
15	2.0×10^3	40	1.3×10^4
16	2.3×10^3	41	1.3×10^4
17	2.6×10^3	42	1.4×10^4
18	2.9×10^3	43	1.4×10^4
19	3.2×10^3	44	1.5×10^4
20	3.6×10^3	45	1.5×10^4
21	3.9×10^3	46	1.6×10^4
22	4.3×10^3	47	1.6×10^4
23	4.6×10^3	48	1.7×10^4
24	5.0×10^3	49	1.7×10^4

TABLE 1, CONTINUED

Latitude in Degrees	Vel (cm s^{-1})	Latitude in Degrees	Vel (cm s^{-1})
50	1.8×10^4	60	2.3×10^4
51	1.8×10^4	61	2.3×10^4
52	1.9×10^4	62	2.4×10^4
53	1.9×10^4	63	2.4×10^4
54	2.0×10^4	64	2.5×10^4
55	2.0×10^4	65	2.5×10^4
56	2.1×10^4	70	2.7×10^4
57	2.1×10^4	75	2.8×10^4
58	2.2×10^4	80	2.9×10^4
59	2.2×10^4		

where J is the current, $\mathcal{L}$ is the unit length inductance, A is the cross-sectional area, and ℓ is the prominence length. Then

$$J \frac{dJ}{dt} \mathcal{L} \ell = \frac{d\ell}{dt} \left| \frac{B^2}{\mu_o} A - \frac{1}{2} J^2 \mathcal{L} \right| .$$

If δ is defined as the angle from the local meridian, then $v_s \sin\delta = d\ell/dt$, the change in the prominence length with respect to time as the footpoints are stretched due to the relative velocity. Then

$$\frac{dJ}{dt} = \frac{v_s \sin\delta}{J \mathcal{L} \ell} \left[\frac{B^2}{\mu_o} A - \frac{1}{2} J^2 \mathcal{L} \right] . \qquad (1)$$

As the rate of current production increases, one would expect shorter lifetimes, and, therefore, a correlation between lifetime and $\ell/v_s \sin\delta$ may exist. The cross-sectional area or the ratio of the cross-sectional area to the length may be other possible predictors.

2.2 Observational Procedures

The first procedure was to review and sketch prominences from 35mm H-alpha patrol film obtained from the U.S. Department of Commerce, World Data Center A (Figure 1) in order to measure lengths, tilt angles, and widths of the prominences. This method proved extremely time-consuming, and the possibility of missing one prominence while viewing another was a major

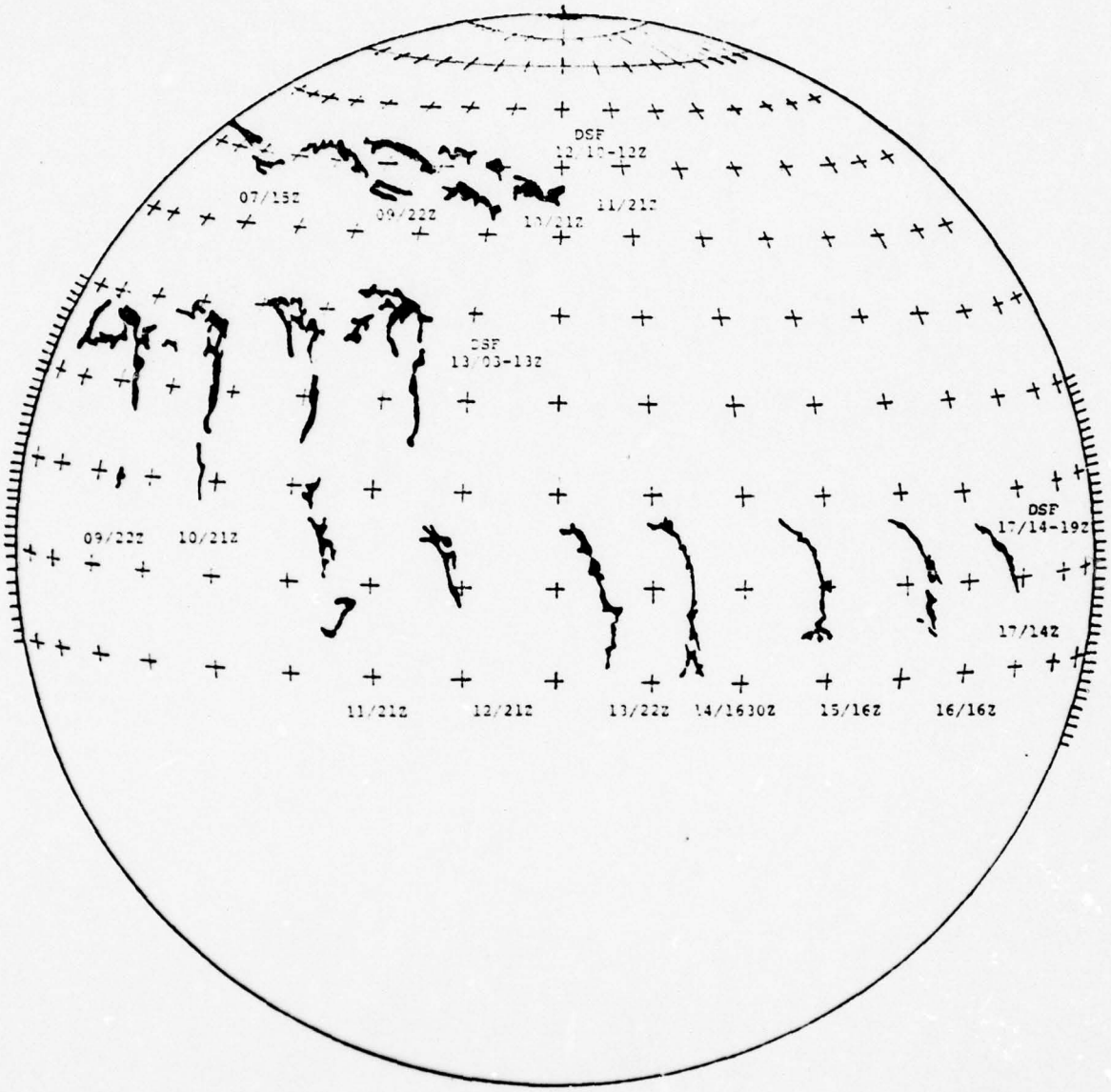

FIGURE 1. Sketches of prominences transiting the disk from H-alpha patrol film projections. (a) Disappearing Sudden Filament (DSF) occurred on 12 July 1973. (b) Partial DSF on 13 July and total DSF on 17 July.

difficulty in using the motion analyzer to correlate lifetimes to the various predictors. Analysis of Fraunhofer Maps proved faster and much more efficient from a statistical point of view. Prominences and filaments were traced on a daily survey by the Fraunhofer Institute and so could be used to trace lifetimes in 24-hour intervals (Figure 2). Comparisons between these and the Solar-Geophysical Prompt reports published by the U.S. Department of Commerce were then used to determine the proximity of the filaments to active regions and to check H-alpha photographs of the disk to verify the Fraunhofer drawings. From Mt. Wilson magnetograms, the magnetic field in the vicinity of the filaments was determined. The sample consisted of those filaments outside of active regions that were seen on the east limb or that originated within approximately 20 degrees of the limb and traversed the entire visible disk, and those filaments that originated and erupted on the visible disk.

Filaments that rotated around the east limb and erupted on the visible disk, and those that originated within the visible disk and rotated behind the west limb were not considered since the history on the far side of the disk could not be determined. During 1973, 83 cases of filaments were found that had lifetimes greater than one day and lengths of five degrees or more.

(a) 7-20 April 1972

(b) 23 March 1972 - 4 April 1972

FIGURE 2. Filament lifetime examples sketched from Fraunhofer Maps. (a) Transit time across disk from 7 April to 20 April 1972. (b) Transit time across disk from 23 March 1972 to 4 April 1972.

Filaments that did not meet this criteria were considered too transient to be quiescents. Those filaments with greater than 8-day lifetimes were then considered as the more stable group and those with less than 8 were considered the more unstable group.

2.3 The Results

The parameters were tabulated in Table 2. Lengths of the filaments were also plotted against lifetimes; a typical graph is shown on Figure 3. The lengths were estimated in degrees by using the coordinates of the end footpoints that could be seen in projection against the disk. These graphs generally showed three types of progressions. One occurred in which the filament length varied slightly during disk passage. Another type seemed to have lengths that varied slightly for a period followed by a large increase in the length and then partial or total eruption. The third type apparently had an increase in length followed by a small period of stability and then partial or total eruption, or a lengthening followed by eruption with no intervening plateau. The latter type seemed shorter-lived and did not attain long lengths (Figure 3).

Figure 4 shows a plot of the lengths of the filaments and their lifetimes. Long-lived filaments appeared to have any length varying from five degrees

TABLE 2

EXAMPLES OF PROMINENCE LIFETIMES FOR 1973

Date	Coord.	Max. Length in Deg.	Life-time in Days	Tilt^{o}	sinδ/ℓ	Neutral Line Rotation No.	Coronal Hole Occur.	Eruptive Occur.	Activity	Width to Length Ratio at CMP
JAN 1	S22E55	20	>13	72	0.05	-	no	no	no	0.10
JAN 5	N22E75	7.6	>12	53	0.10	-	yes	no	no	0.40
JAN 6	S05E27	11.6	<3	-49	--	-	yes	yes	slight	0.13
JAN 6	N35W15	18	<3	63	0.05	-	no	yes	slight	0.06
JAN 5	S19 EL	6.5	>14	59	0.13	-	no	no	slight	0.25
JAN 6	S08E78	22	>13	55	0.04	-	no	no	mod	0.13
JAN 14	S05W12	18	>12	8	0.01	-	no	no	slight	0.05
FEB 3	S25W15	25	>13	53	0.03	-	no	no	slight	0.03
FEB 5	N35E12	5.7	<6	79	0.17	-	yes	yes	no	0.08
MAR 1	N20E17	18	>12	18	0.02	-	no	no	mod	0.06
MAR 12	S27 CM	55	>14	54	0.015	-	no	no	slight	0.03
APR 4	S08 CM	19	>16	90	0.05	-	no	no	no	0.10
MAY 1	S10E05	27	>12	90	0.04	2	no	no	mod	0.09
MAY 8	S08E10	6	<2	0	0	2	no	yes	mod	0.06
MAY 10	S22W08	7.2	<9	31	0.07	6	no	yes	mod	0.14

TABLE 2, CONTINUED

Date	Coord.	Max. Length In Deg.	Life-time in Days	Tilt°	sinδ/ℓ	Neutral Line Rotation No.	Coronal Hole Occur.	Eruptive Occur.	Activity	Width to Length Ratio at CMP
MAY 17	N07E25	6.3	<2	72	0.15	1	no	no	slight	0.10
MAY 23	N15W05	32	>14	32	0.02	6	no	no	slight	0.10
JUL 13	00 E02	14.5	<8	23	0.03	4	no	yes	slight	0.13
JUL 19	N23 CM	20	>12	76	0.05	6	no	no	slight	0.05
JUL 24	S15W07	16.8	<7	20	0.02	2	yes	yes	mod	0.03
JUL 31	N32E40	5.8	<3	59	0.15	1	no	yes	no	0.20
AUG 9	N20E03	13	>13	34	0.04	5	no	no	slight	0.06
AUG 18	S03W03	16.8	>16	-50	-	6	no	no	mod	0.08
SEP 5	N38E35	8	<4	90	0.125	2	no	yes	no	0.13
SEP 13	S10E05	7	<5	16	0.04	4	no	yes	slight	0.25
OCT 2	N20E03	11.6	>9	76	0.08	6	yes	no	slight	0.14
OCT 7	S20E02	5	<3	79	0.20	11	yes	yes	slight	0.17
OCT 22	S07W07	7	>14	37	0.09	7	no	no	no	0.17
OCT 27	N30 CM	19	>11	0	0	3	yes	yes	no	0.30
OCT 23	N38 CM	15.8	>14	-69	-	6	yes	no	no	0.03
NOV 2	N10W03	13	>14	28	0.04	10	no	no	no	0.10
NOV 7	N15 CM	10	>14	69	0.09	2	no	no	slight	0.20
NOV 26	N40W05	25	>16	41	0.03	4	yes	no	slight	0.15

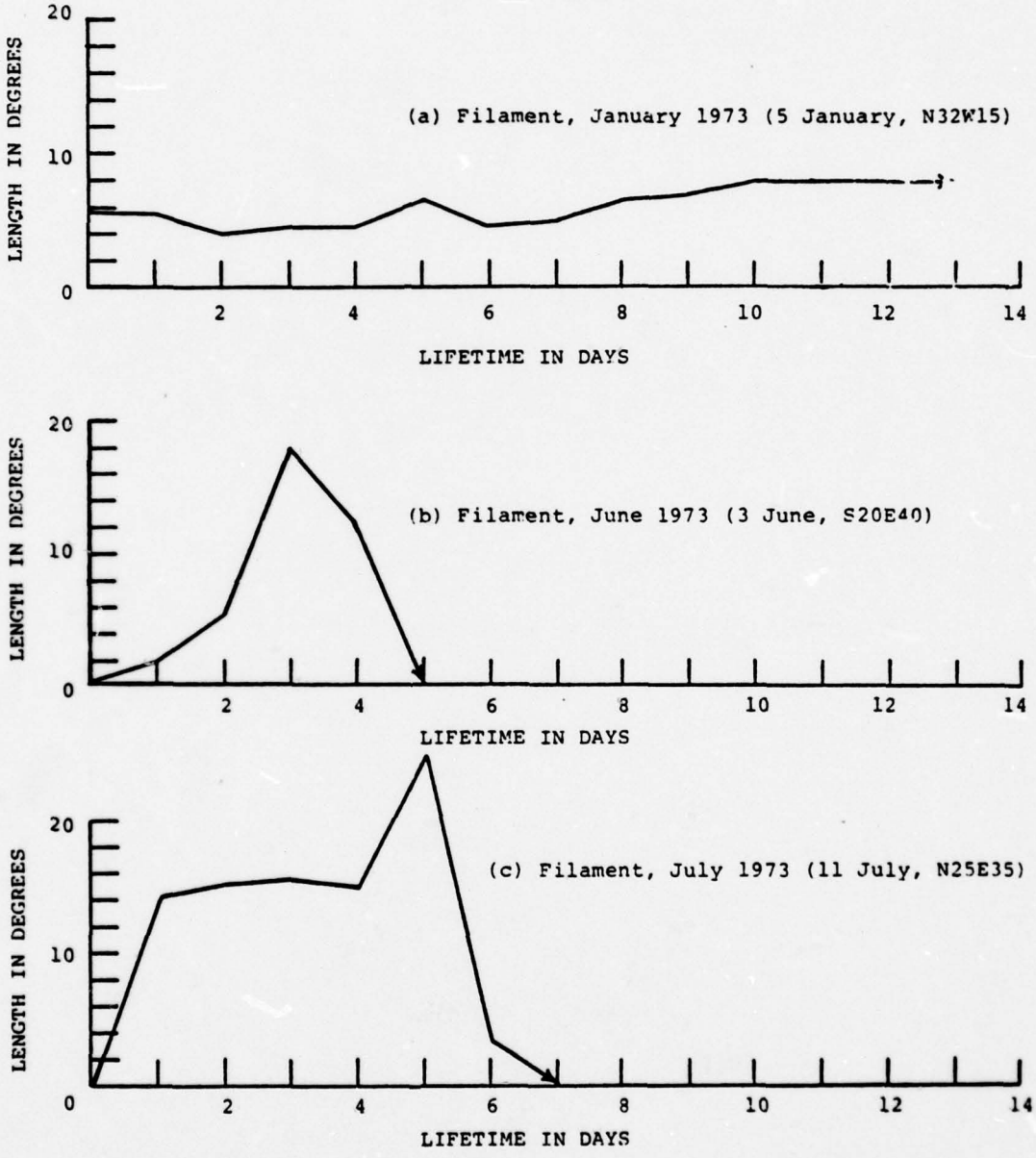

FIGURE 3. Typical lifetime vs. length characteristics of prominences.

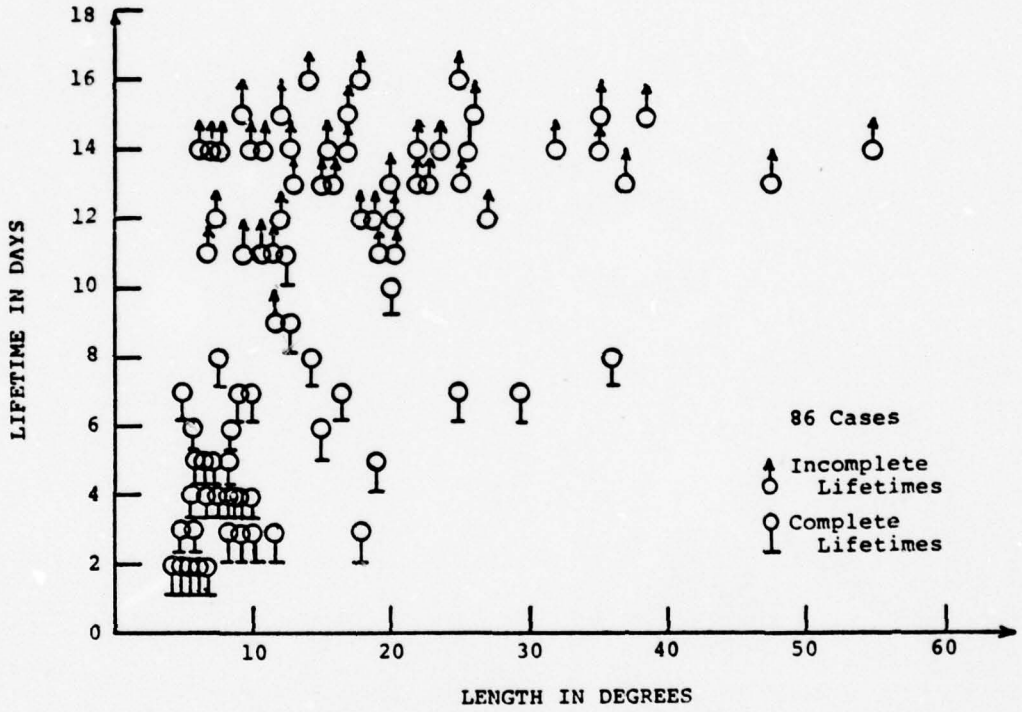

FIGURE 4. Length vs. lifetime prominence characteristics in 1973.

to fifty-five degrees. There was an indication that the longest filaments had long lifetimes and that very short filaments generally had short lifetimes (Figure 4). This relation implies that there is a certain growth time required for the filaments to attain greater visible lengths.

The ratios of the $\sin\delta/\ell$ to the lifetimes appear to be related. The tilt angle was measured at Central Meridian Passage (CMP), if possible, to reduce foreshortening. Filaments that were in areas where the H-alpha photographs showed plage brightening, and the magnetograms showed magnetic fields greater than five Gauss and were removed from this sample to minimize any effects of emerging or changing photospheric flux. The results were that 77% of the data were within quadrants I and IV (Figures 5 and 6). Quadrant I was associated with long-lived, stable filaments and low $\sin\delta/\ell$ ratios. Quadrant IV contained short-lived filaments and high $\sin\delta/\ell$ ratios. The percentage of cases increased from 71% to 77% within Quadrants I and IV when the filaments that may have been affected by emerging flux regions were removed. This six percent decrease in the scatter indicates that changing photospheric flux probably decreases prominence stability as expected. This is further shown by the percentage of long-lived filaments to the total which increased from 58% to 61% after those

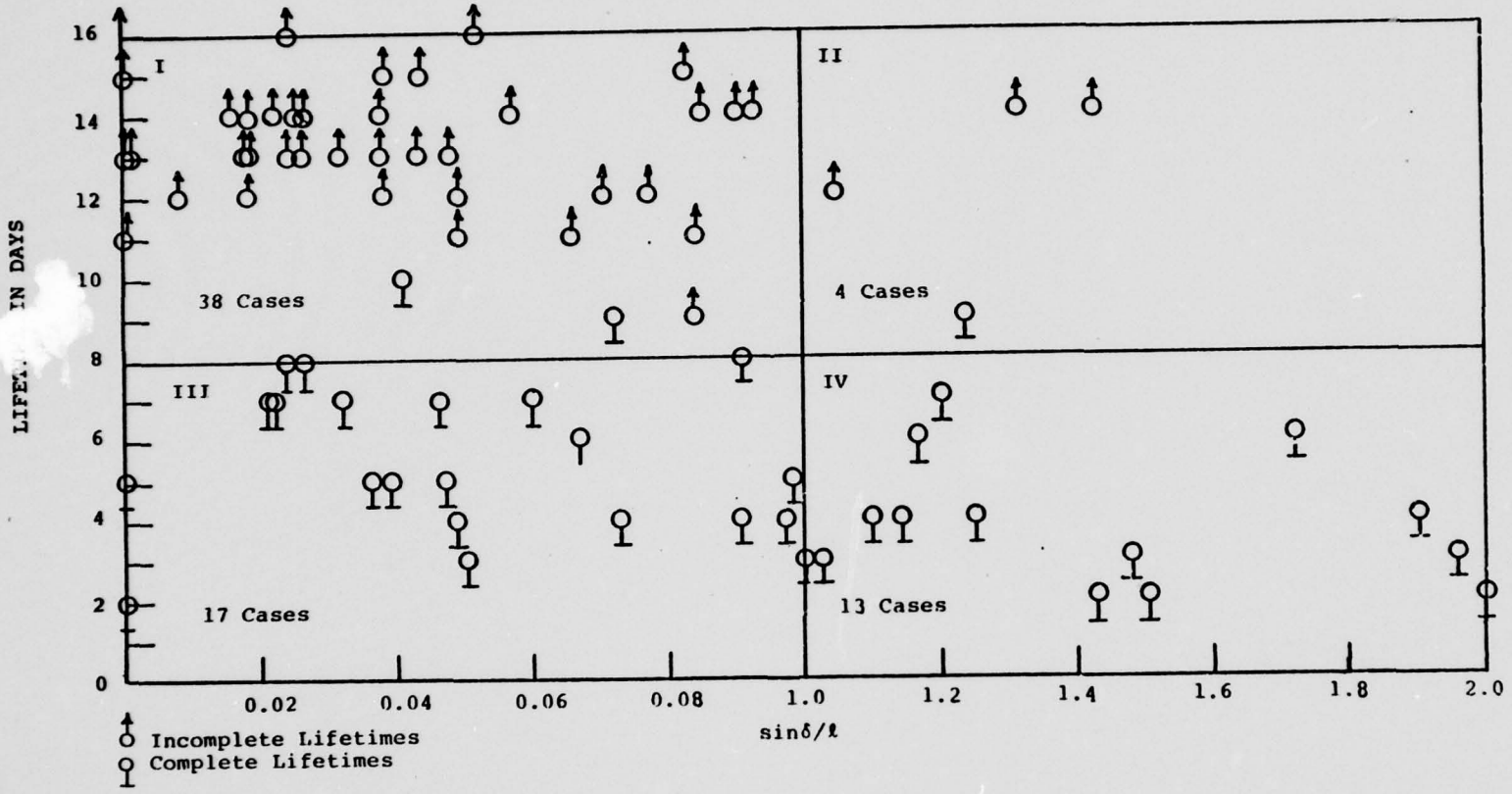

FIGURE 5. Sine tilt angle-to-length relationship to prominence lifetimes for 1973.

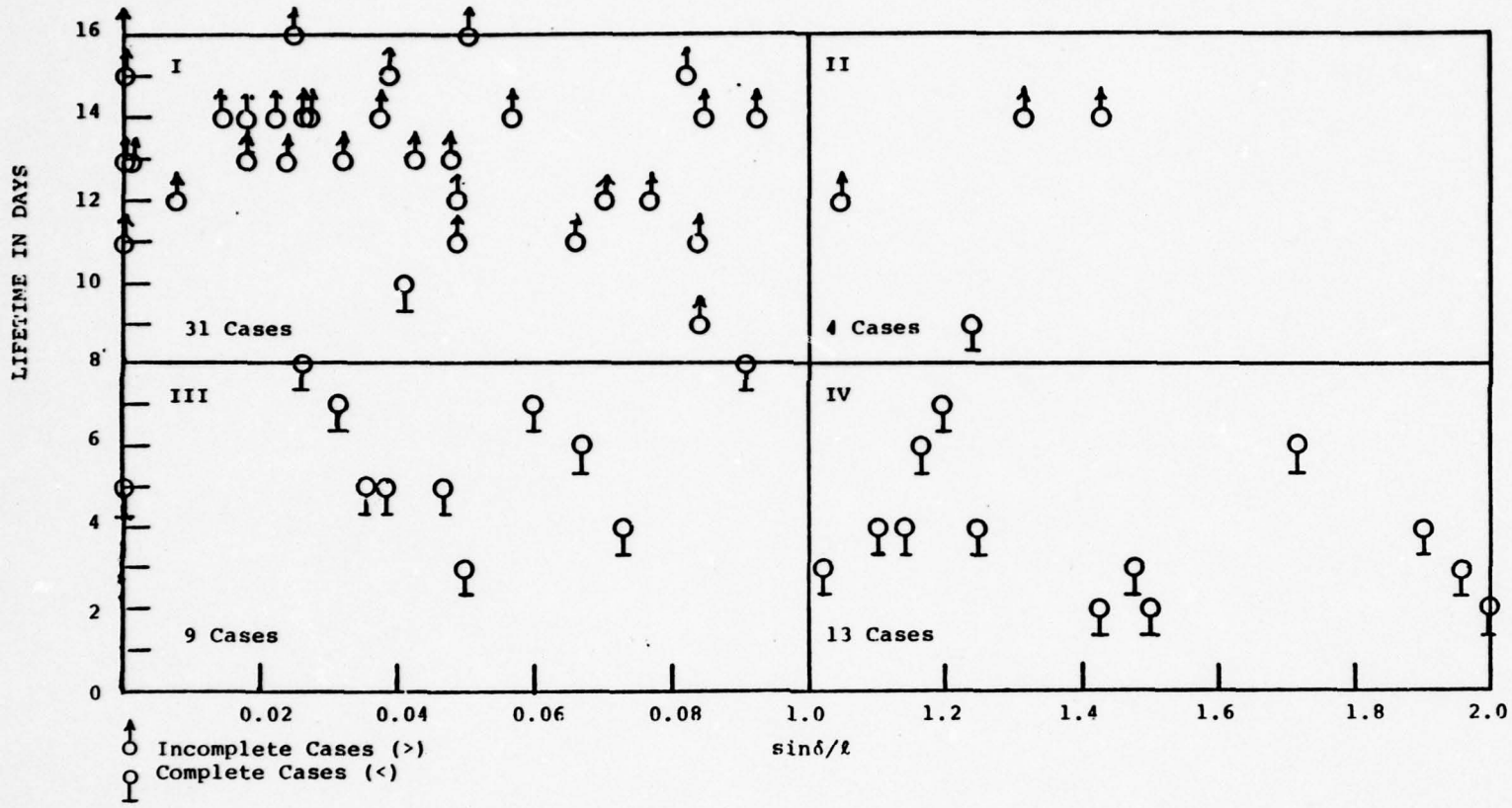

FIGURE 6. Sine tilt angle/length of prominences to lifetimes for 1973. Those cases which might be associated with emerging flux areas are removed.

filaments associated with emerging flux were removed. No correlation was found when only the tilt angles of the prominences were plotted against lifetimes (Figure 7).

To investigate the correlation of the area-to-length ratio to lifetimes, a constant prominence height was assumed, ratios of widths to lengths were computed, and then compared with lifetimes. The width-to-length ratios were estimated at CMP to reduce errors from foreshortening. The assumption of constant height is not necessarily good since different prominences may be of different heights. No correlation was found between these ratios and lifetimes (Figure 8). The width-to-length ratios were found to have a mean of 0.13 with a standard deviation of 0.1; this means that average widths would vary from approximately 3000 km to 23,000 km for prominences of 100,000 km in length. This seemed somewhat high. In isolated cases, some prominence observations showed large, distinctive eruptives which appeared to be wider than is normally observed. Most cases occurred close to limbs, and the widths may have in reality been the heights of the prominences observed against the disk because of the solar curvature. A possible relationship between heights and eruptives is suggested and should be studied. If footpoints are pulled apart due to their relative motions and the

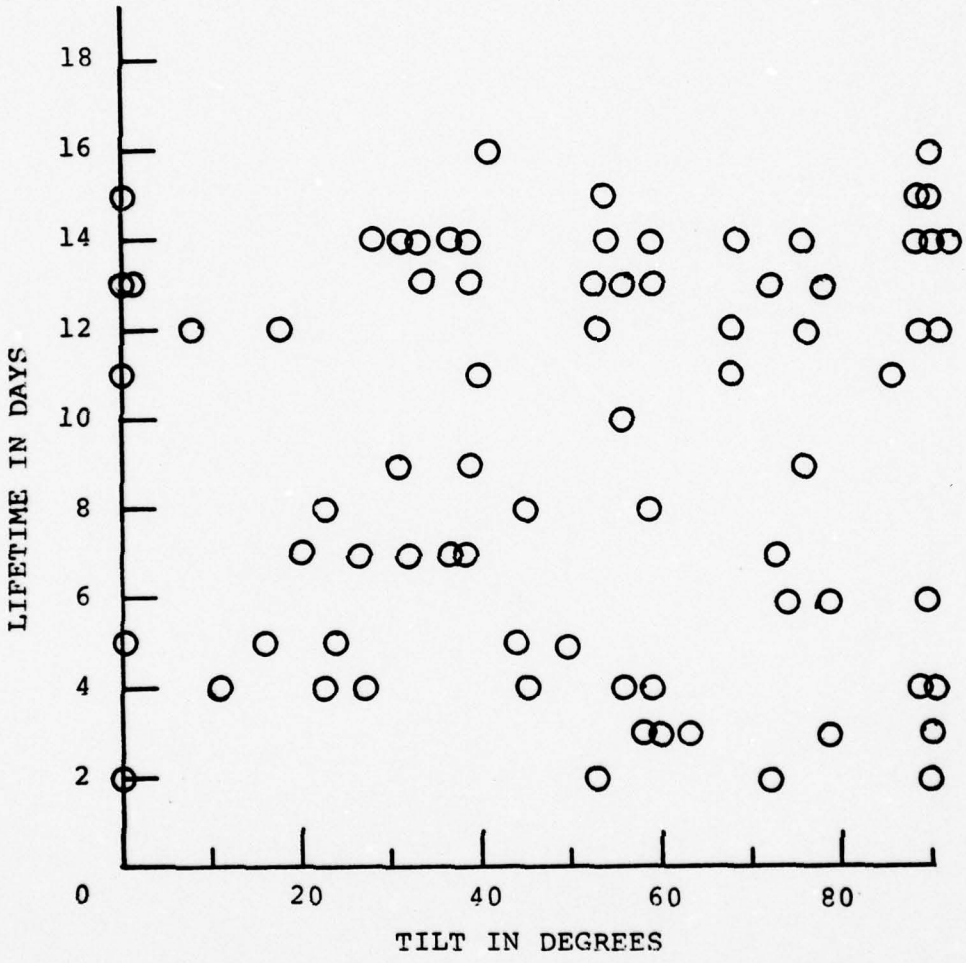

FIGURE 7. Tilt angle vs. lifetime characteristics for prominences in 1973.

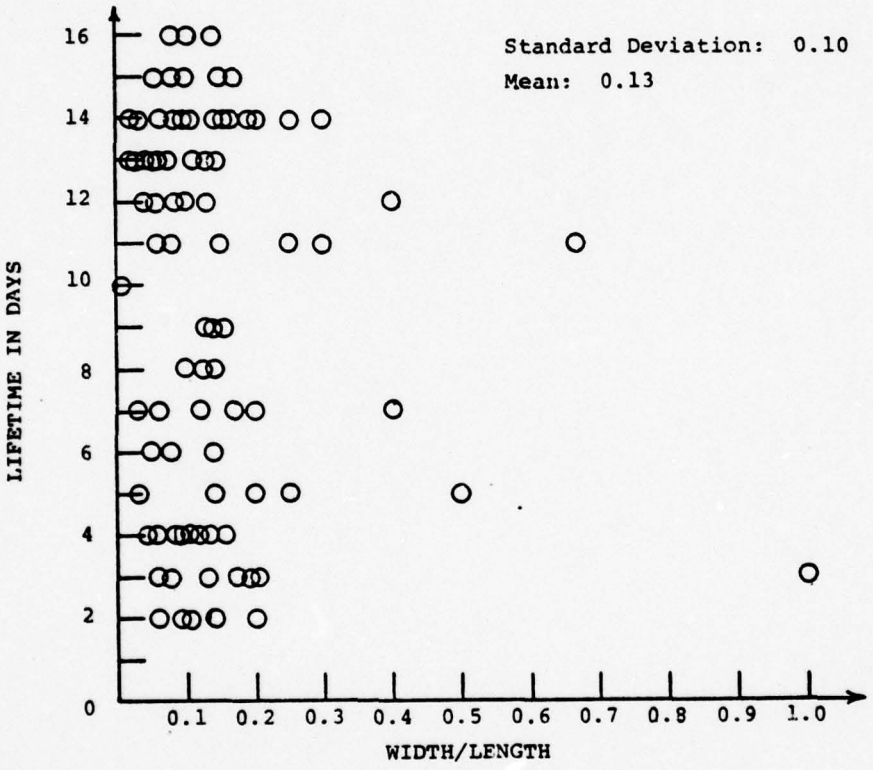

FIGURE 8. Width/length vs. prominence lifetimes in 1973.

prominence height increases as might be expected, then higher prominences may be indicative of current strengths within the prominences and a measure of their instability. Thompson and Billings (1967) have made observations that support the Kippenhahn - Schluter theory that the ratio of the maximum stable height (Z) of a prominence is a function of the distance (D) from its base to the origin of the supporting magnetic field, or $Z/D \simeq 1/3$.

In studying prominence-related x-ray coronal cavities, Serio and Vaiana (1978) found a correlation between the lifetimes of visible prominence elements and the age (in rotations) of neutral lines associated with the x-ray cavities. The age of the neutral lines was based on work by McIntosh (Figure 9). They found that prominence element lifetimes were shorter for neutral lines of ages less than four rotations and greater than ten rotations (new and old neutral lines), and longer lifetimes were found for neutral lines of four to seven rotations (Figure 10). This indicates that a period of growth and decline of neutral lines is accompanied by periods of instability and that stability exists between those periods. In an independent study of the age of neutral lines versus lifetimes, evidence to support the work of Serio and Vaiana was found (Figure 11). There is probably then a stable period for neutral lines associated with prominences. The

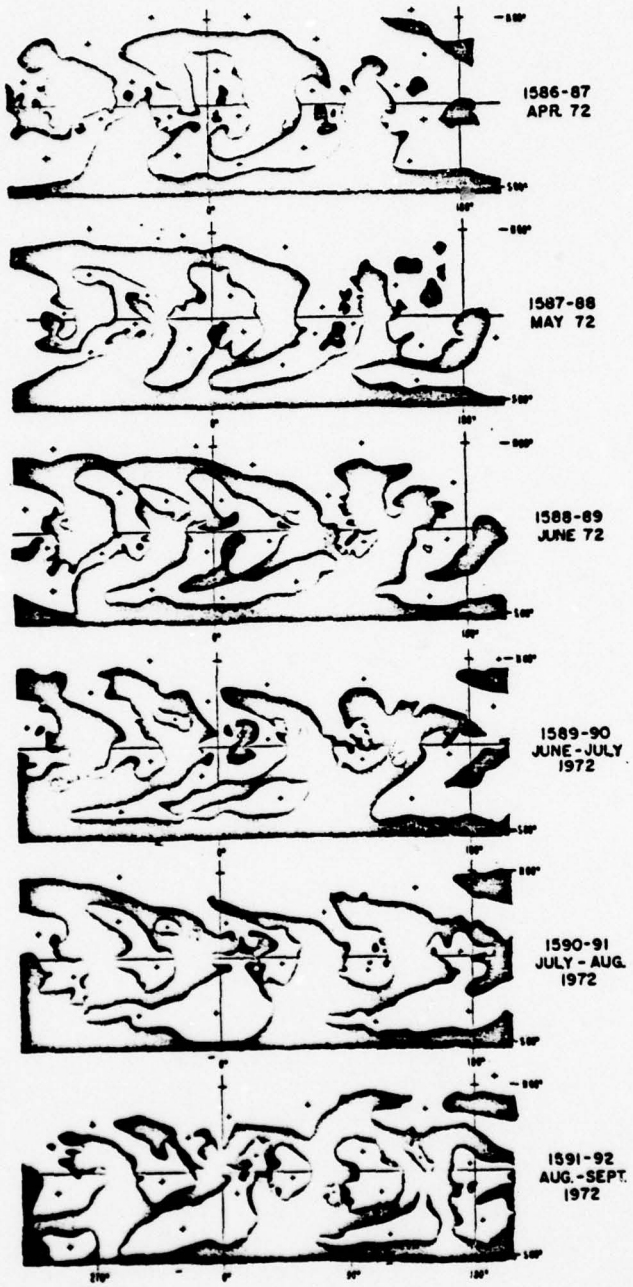

FIGURE 9. H-alpha synoptic charts for rotations 1586-1592. (Courtesy of P. S. McIntosh.)

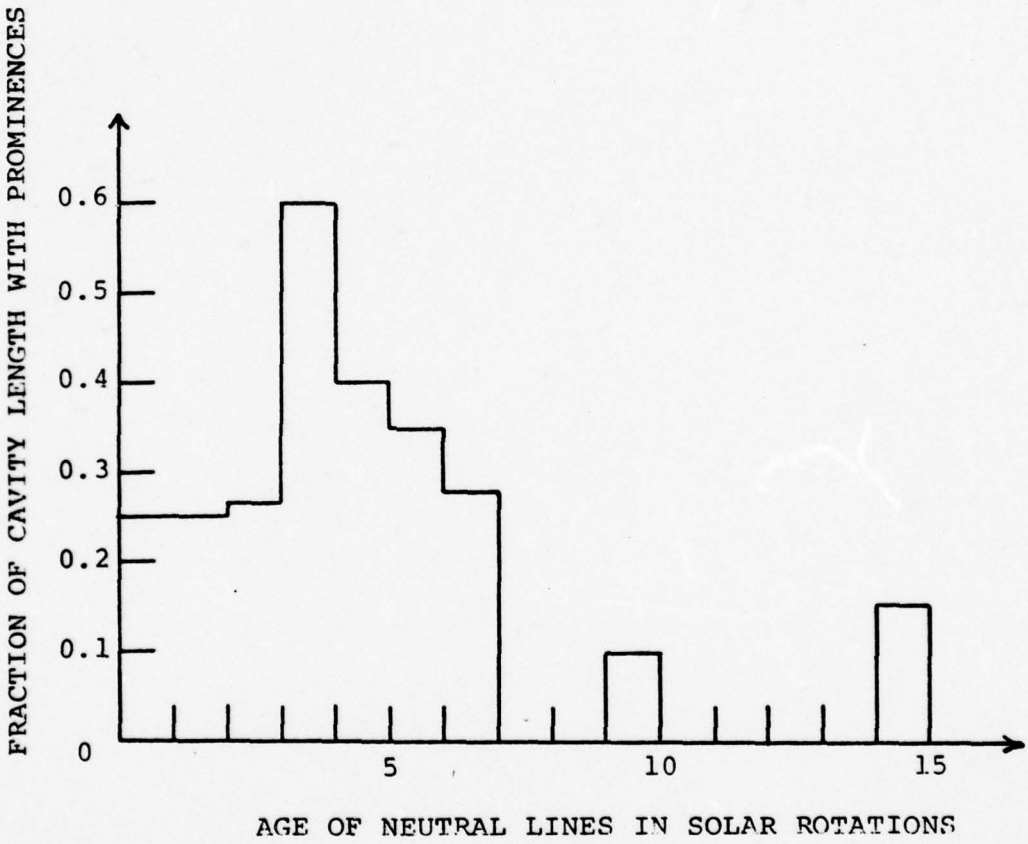

FIGURE 10. Prominence element stability as a function of neutral line age. (Reproduced from Serio, et al., 1977.)

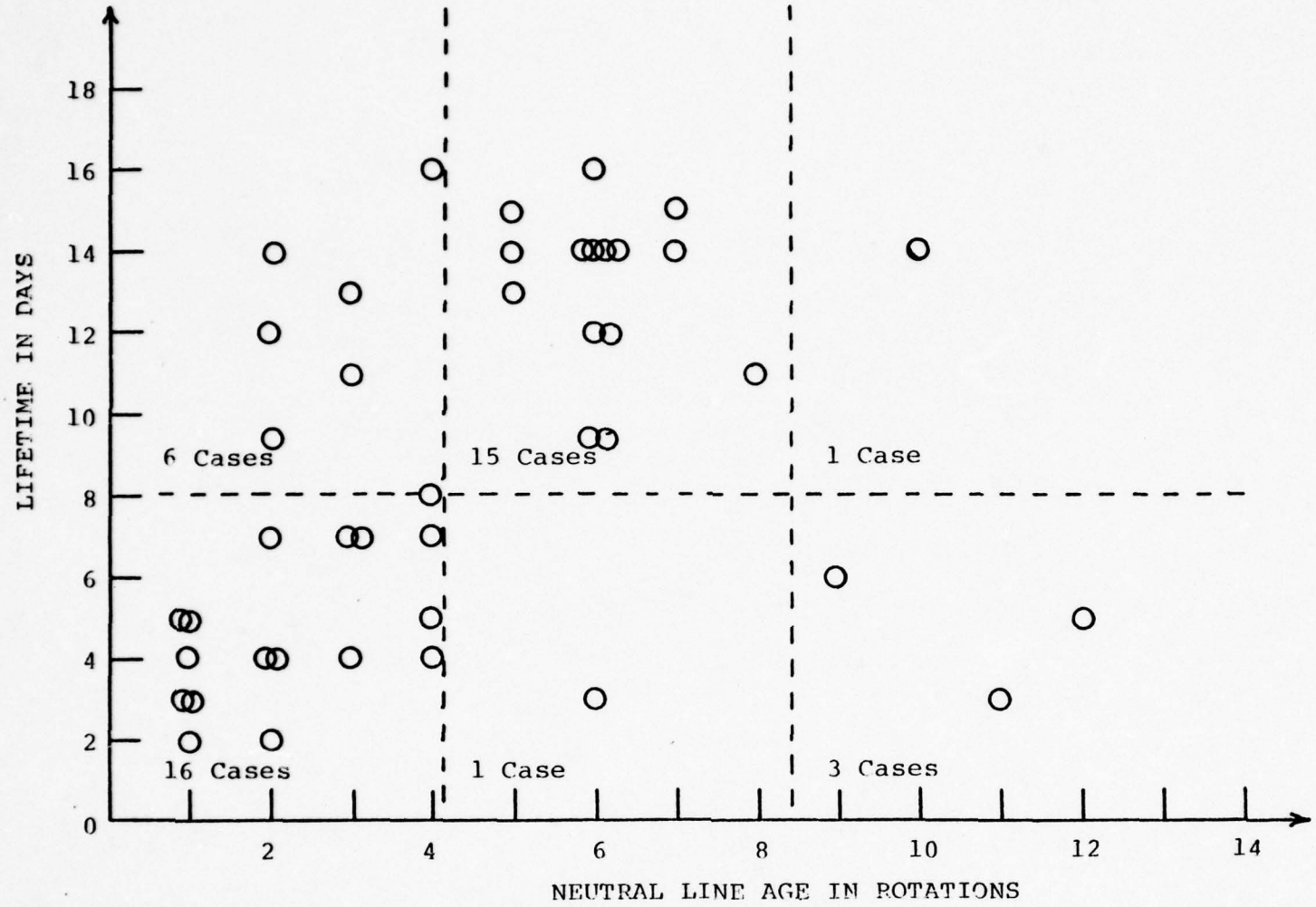

FIGURE 11. Age of neutral lines *vs.* prominence lifetimes for 1973.

relationship between the ratio of $\sin\delta/\ell$ to lifetimes for only those prominences that lie along neutral lines with rotational ages of from four to eight, apparently is also valid. The percentage of prominences in quadrants I and IV increased to 82% of the total number; prominences with lifetimes greater than eight days (quadrants I and II) compared to the total number increased from 61% to 72%. Effects of the coronal fields could account for some of the remaining scatter in the diagrams (Figure 12). The age of the neutral lines were found from "H-alpha Synoptic Charts for Rotations" (McIntosh, private communication) and was difficult to trace. McIntosh (1976) based the initial locations of neutral lines upon several variables, such as prominence locations, filament channels, fibrils, and others. These locations were somewhat open to interpretation. It was difficult to accurately determine the time of origin of a particular neutral line.

Neutral lines bordering coronal holes were found in several ways. Coronal holes were inferred by correlating the H-alpha Rotation Charts with Fe XV, 284Å, x-ray emission measured by OSO-7 reported in the "Solar-Geophysical Prompt Reports." Also, a very good list of coronal holes during the Skylab Workshop period was compiled by Bohlin (1977). When the coronal hole associated prominences were removed, the percentage of

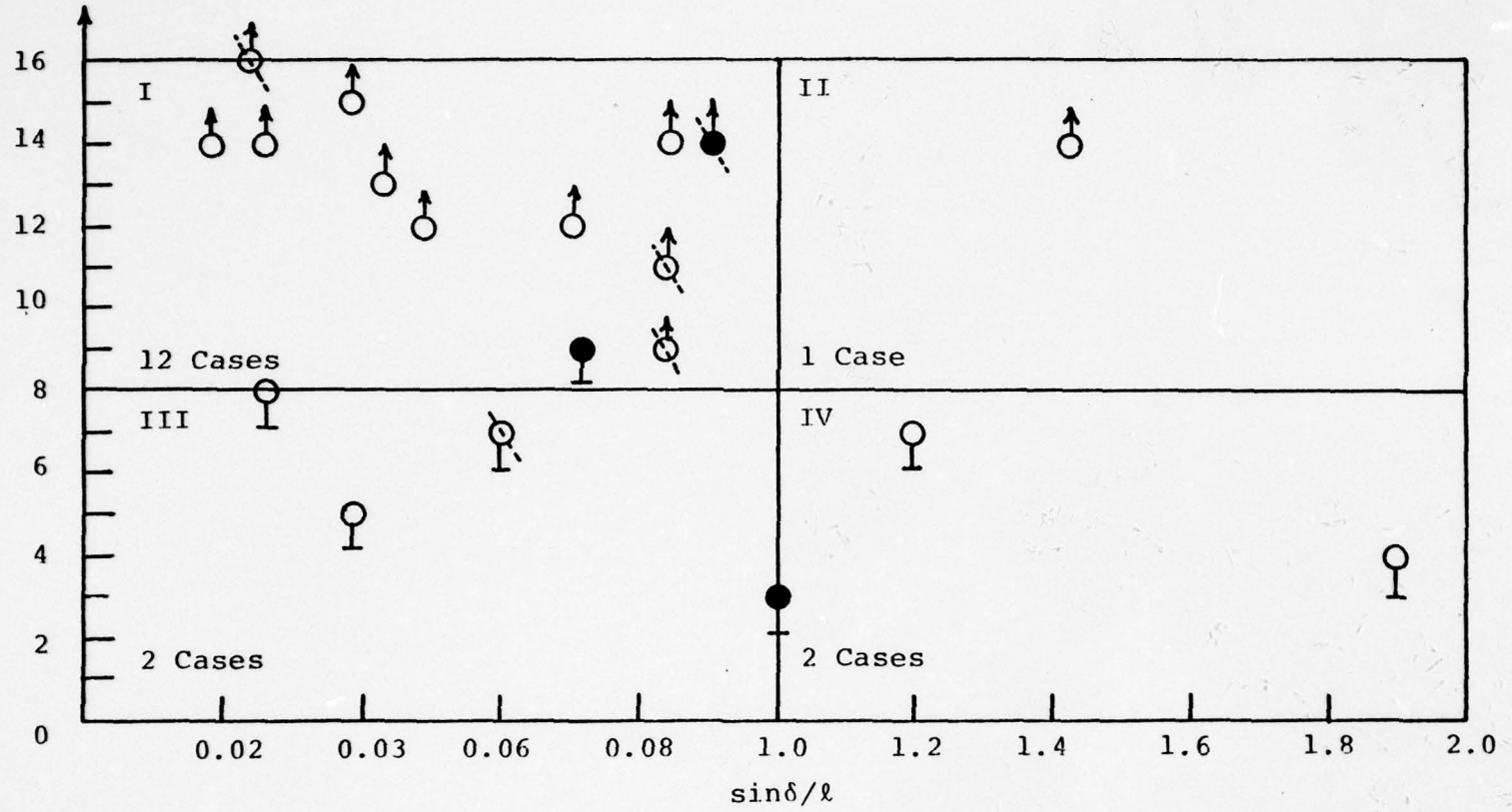

FIGURE 12. Sine tilt angle/length to prominence lifetimes for 1973. (For neutral line rotational lifetimes of 4-8.) ⊙ Coronal hole association. ● Active region association. ↑○ Incomplete lifetimes. ○ Complete lifetimes.

long-lived, stable prominences compared to the total improved from 61% to 64%. This seemed to indicate instabilities in prominences bordering coronal holes (Figures 13 and 14).

If one considers only prominences bordering coronal holes, the $\sin\delta/\ell$ to lifetime relationship still seems valid with 73% of those prominences falling within quadrants I and IV.

A smaller sample from 1971 showed similar results; i.e., there was no apparent relation between the tilt angle and lifetimes, and no correlation was found between lengths and lifetimes, although the lengths were measured only by difference in latitudes $(\phi_1 - \phi_2)$ for the 1971 data. A relationship was apparent, however, for the $\sin\delta$ to length ratios and the prominence lifetimes (Figure 15).

2.4 Summary

The results indicate that a field-aligned current may flow in prominences because of photospheric differential rotation. This current is probably due to stretching of the footpoints as evidenced by the $\sin\delta/\ell$ ratio that equation (1) implies, and which is apparently in agreement with the observed decrease in lifetimes with the increase in this ratio. Prominences are also affected by other mechanisms that cause instabilities.

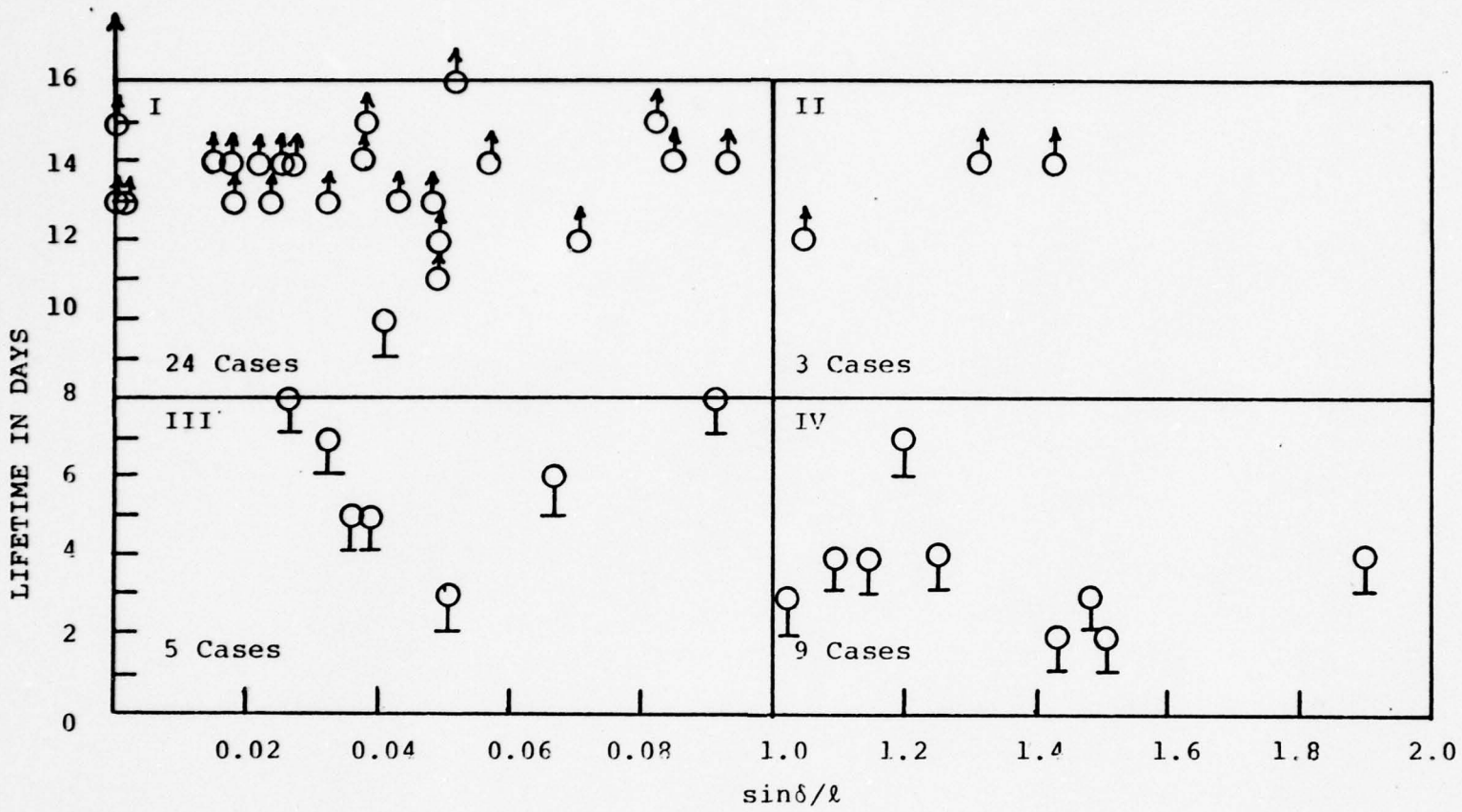

FIGURE 13. Sine tilt angle/length to prominence lifetimes for 1973. (Coronal hole and active association cases removed.) ♂ Incomplete cases. ♀ Complete cases.

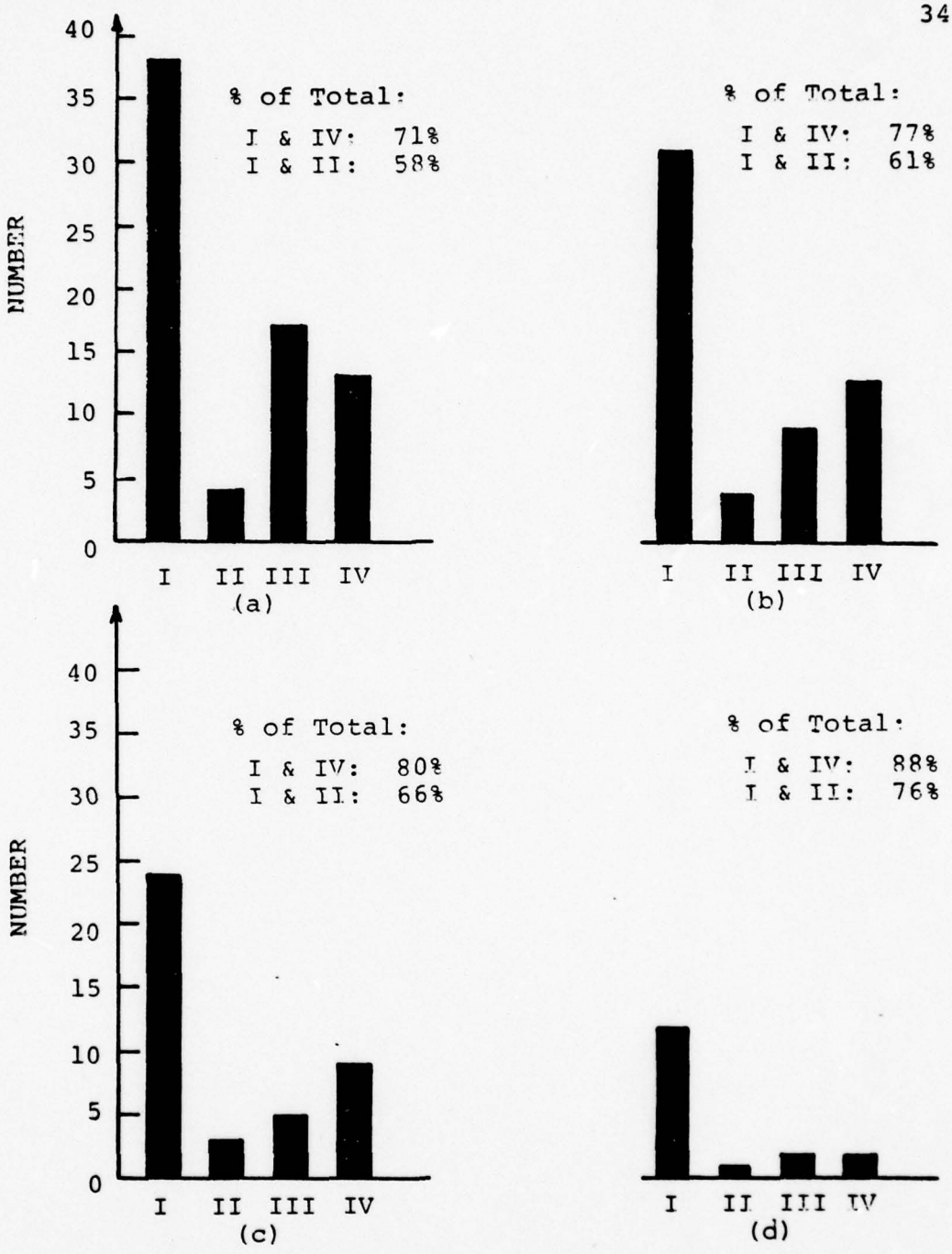

FIGURE 14. Sine tilt angle/Length vs. lifetimes of prominences, histograms for 1973. Quadrant I: high stability, low $\sin\delta/\ell$. II: high stability. high $\sin\delta/\ell$. III: low stability, low $\sin\delta/\ell$. IV: low stability, high $\sin\delta/\ell$. (Data from Figs. 5, 6, 12, and 13.) (a) Quadrants (all) from Figure 5. (b) $\sin\delta/\ell$ diagram quadrants (active cases removed) from Figure 6. (c) Quadrants (active cases removed and coronal hole association prominences removed) from Figure 13. (d) Quadrants 4-8 rotation group from Figure 12.

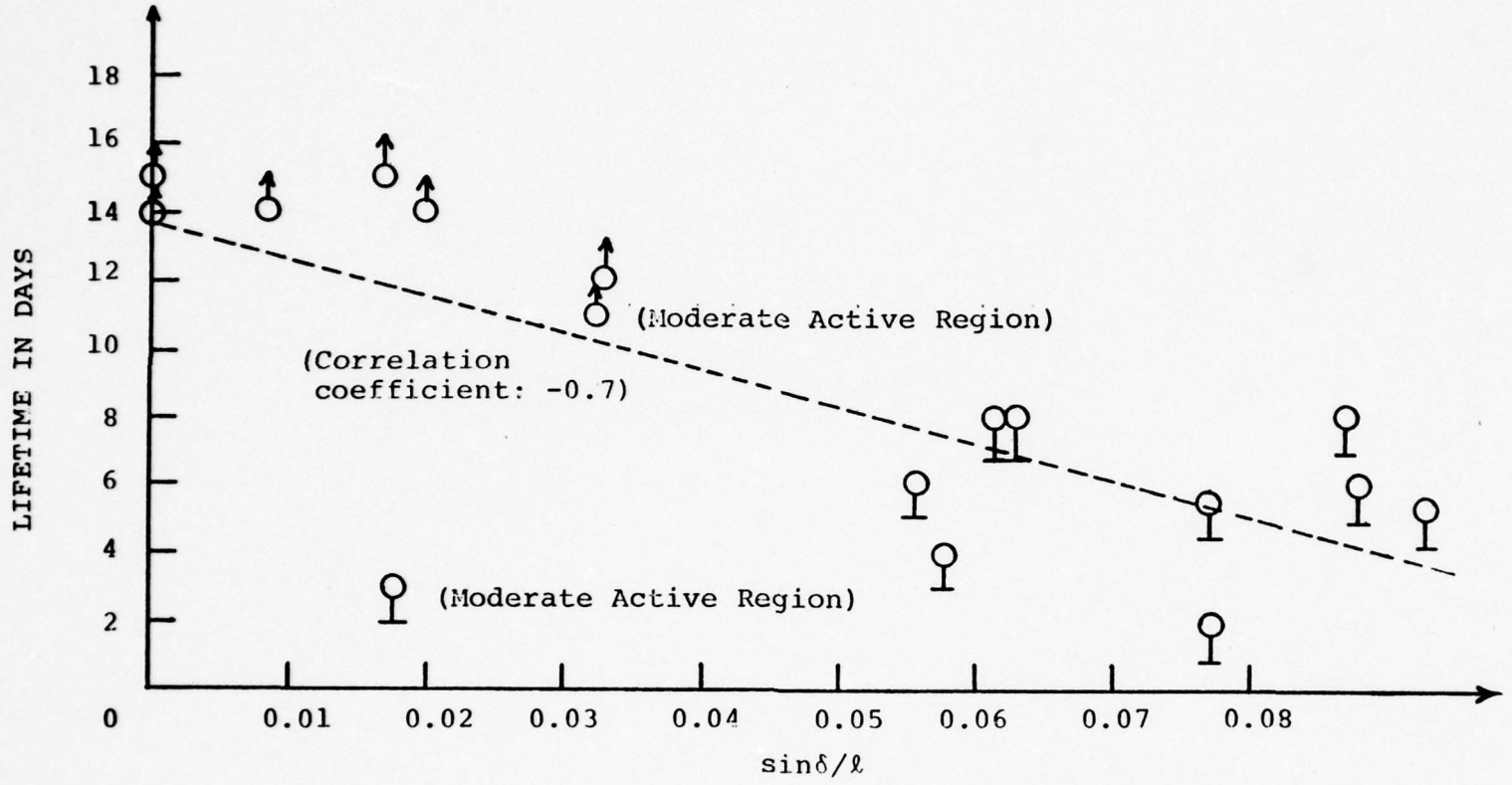

FIGURE 15. Sinδ/length vs. lifetime characteristics of prominences in 1971. Complete lifetimes. Incomplete lifetimes.

These could be emerging flux regions or effects of the overburdening coronal fields, as the coronal hole boundary study may imply. If most of the field lines in coronal holes are open, then one might expect a smaller overlying closed field with respect to the prominences, and, therefore, a smaller eruptive energy would be required by the prominence to overcome this coronal field. However, another explanation for instabilities due to coronal holes should be mentioned in view of the Kippenhahn-Schlüter model of prominences: a prominence bordering a coronal hole could not have the multipole fields on both sides of the prominence to provide the configuration required to support it (Kippenhan-Schlüter, 1957). This raises questions about the initial formation of the prominence along the coronal hole before the eruption.

CHAPTER III

FLARE ASSOCIATED λ5303 ANGSTROM CHARACTERISTICS

3.1 Coronagraph Coronal Stability

The λ5303 Å, Fe XIV, coronal filtergrams are monochromatic survey films that were taken once a day during the period 1956 to 1974. The instrument was a 6-inch coronagraph containing a λ5303 Å birefringent filter with a two-Angstrom bandpass located at Sacramento Peak Observatory. The solar limb was photographed in 60 degree sectors showing green line emission of FE XIV, which delineates the lower coronal magnetic structures (about 1.04 to 1.2 solar radii). These magnetic structures are quasi-stable and although fast transients are sometimes observed, the corona usually returns to its pre-transient configuration (DeMastus, et al., 1973). This feature of quasi-stability allows one to observe the properties of the lower corona during limb passage with the inference that the coronal magnetic configuration would not be appreciably altered within a few days. If one is fortunate enough to observe a limb flare during the passage of an active region, the green line filtergrams should show the basic general

configuration of the corona above the flaring region. A dramatic example of this which is discussed by Dunn can be seen in the flare-associated green line coronal loops which apparently form sheaths over H-alpha loop prominences (Dunn, 1971). If a flare occurs within a few days of limb passage, the east limb filtergram should show the pre-flare lower coronal magnetic configuration as inferred from Fe XIV. Since the current view of many solar physicists is that flare and flare-like events have their origins in the lower corona, where densities are less and magnetic reconnections and field annihilation rates are more feasible, a study of the characteristics of east limb features and their correlations with H-alpha regions which are just entering the visible disk might be important to further the knowledge of flare morphology. There is an added advantage that if flare related features were found in the λ5303 filtergrams, they might also prove useful in providing flare prediction parameters. Studies of the west limb coronal features might be useful in understanding post-flare activities, but this was not attempted here.

3.2 Observational Difficulties and Terminology

In order for one to interpret the green line corona properly, the difficulties and limitations in obtaining

photographs must be understood and some standardization in terminology must be attempted. The corona is very faint. The brightness of the green line varies between 10^{-5} and 2×10^{-4} of the intensity of the photospheric continuum, while the maximum sky brightness for which this coronagraph can operate is about 50×10^{-6} of the disk. Sky brightness and fluctuations from particulates in the earth's atmosphere result in an extreme brightening of the sky which results in flashes and reductions in contrast. Since the width of the green line is three-fourths Angstroms and the birefringent filter is two Angstroms, the ratio of the green line intensity to that of the scattered light continuum transmitted by the filter is low, reducing the contrast. When the faintness of the green line is coupled with low transmission filters, one or more minutes are necessary for proper exposure (Dunn, 1971). These limitations result in very low contrast which makes observations and photography difficult. Because of guiding errors and changes in seeing, underocculting sometimes occurs, resulting in sudden brightenings within these long exposures. Resolution is then relatively poor due to the long exposures and also appears fuzzy from the diffuse coronal structures which are dilated in comparison with chromospheric structures (Dunn, 1971; Frankenthal, 1976). Since the background

brightness varies so much, the exposures must be continually changed in order to obtain the faintest details. It is therefore almost impossible to obtain density standards and consequently difficult to interpret intensities. Another important limitation that must be taken into account is the optical thinness of the corona. Several regions may be superimposed over one another; the result is increased brightness where the loop of one region crosses the loop of another region along the line of sight. These different features must be disentangled for proper interpretation. For a more thorough discussion of difficulties associated with green line coronal studies, the reader is referred to Dunn (1971), who provides a detailed review of these problems. Terminology used here is also described by Dunn in discussing various structures and features of the corona.

The ionization potential of Fe XIV is 335 eV. Since the high energy tail of the distribution must be considered, the coronal temperature necessary for green line emission is of the order 1.8×10^6 ^{o}K (Jacobs, 1977). The magnetic structure inferred from the green line coronal emission appears as loops, arches, arcades and rays. Arcades, loops, and arches may further be described as "hairpin" shaped or "bridge-like" in appearance, depending on their orientation to the viewer, and

should describe a closed magnetic region. Rays should correspond to open magnetic regions. Dunn (1971) completely describes the characteristics of loops and arches and their differences.

This study centers on the coronal survey film (CSG) for quasi-stable features and does not consider the green line coronal transients. A very comprehensive study of λ5303 coronal transients and H-alpha activity was previously made by DeMastus, Wagner, and Robinson (1973). One of the initial objectives of this study, to observe relative motions between loops in areas wehre reconnection, magnetic field annihilation, and current sheet might occur, was not found to be feasible for several reasons. The resolution in λ5303 was too poor to maintain the identity of the individual loops over any elapsed period and the data was so sparse that there are few cases of consecutive daily frames of the same region. A further problem is that regions approaching, passing the limb, and on the visible disk are foreshortened with resulting changes in the apparent height and general appearance of the region. Slow temporal changes in the green line coronal loops, then, are extremely difficult to obtain. However, indications from other coronal observations are that flares (and by inference field annihilation and current sheets) may begin lower in the corona than can be seen in the

Sacramento Peak λ5303 filtergrams. The occultation from the coronagraph precludes viewing below approximately (22-25) x 10^3 km. Dunn (1971) and DeMastus (1973) conclude from observations of fast transients in the green line corona that violent coronal disturbances begin below at least 25 x 10^3 km. Rust (1977) suggests that there may be two different classes of flares, one that occurs below 10,000 km and is compact and brief with higher energy density, and another that is high (approximately 50,000 km). This suggestion was based on a survey of soft x-ray limb flare images (Pallavicini, Serio, and Vaiana, 1977).

3.3 Observational Procedures

The 1973 observational period was chosen, concentrating on filtergrams of the east limb. λ5303 data and H-alpha activity were correlated by projecting the filtergram upon 15.1 cm Stoneyhurst maps of the corresponding day's activity summary made by the Fraunhofer Institute. This map shows locations of plage regions and prominences/filaments on the disk and limb. The H-alpha flare data was obtained from the "Solar Geophysical Data" (Prompt Reports and Comprehensive Reports) published by the U.S. Department of Commerce. The McMath region associated with a particular λ5303 filtergram was identified by computing the

time of central meridian passage (CMP) of the region, which is approximately 6.8 to 7.0 days from the time of its limb passage. The McMath regions are listed as "Regions of Solar Activity" in the Prompt Reports. Magnetic structure "seen" in λ5303 was checked against Mt. Wilson Magnetograms obtained from the Department of Commerce, World Data Center A, Boulder, Colorado. A comparison of the data should allow one to infer a three-dimensional view of the coronal magnetic structure.

A particularly difficult task before the λ5303 filtergrams could be correlated with H-alpha activity was the parameterization of the coronal features so that an objective study could be made. The parameters that were chosen were the green-line coronal height, intensity of the Fe XIV emission, definition/resolution of features in the coronal region, open or closed magnetic fields, angular extent of the region and percent of coverage of brightness along the angular extent, and the complexity of the magnetic fields in the coronal region. Individual coronal regions were studied for spatial correlation with the latitudinal position of flares that occurred within several days of limb passage. The filtergrams were also examined for any other features that might be associated with flares; i.e., bright, localized areas at the base of tops of the loops or

apparent shearing between loops, which may infer non-potential field configurations and coronal current flow.

The height of the visible green-line corona is an indication of the vertical extent of the density and temperature required for Fe XIV emission. It should be related to the size of the associated chromospheric active regions and may be correlated with flare activity. If, as mentioned by Rust, there are two different flare classes, one of which is low with little coronal impact and the other which is high with greater effects on the corona, then there may be no correlation between flares and green-line coronal heights. There is some error in heights resulting from guiding errors, crudeness in measurement, and faintness of the features; however, the error should be random and the measured heights of the features seem reasonable. These heights ranged from ∿41,000 km to ∿125,000 km. This corresponds favorably with the 1.04 to 1.2 $R_{\odot}$ range found for the green-line corona by DeMastus, et al. (1973).

The brightness of a coronal region should be related to the density and temperature over an active region. Increased emissions have been found in the lines related to highly active regions. The yellow line of calcium, in particular, has shown up in hot spots over the potential flaring areas. Dolder, Roberts, and Billings

(1954) found that the λ5694 yellow line was highly correlated with flares at the Sun's limb. One might expect a correlation between the green line intensity and the activity of the corresponding chromospheric region. There are, however, extreme difficulties in measuring and interpreting this intensity since atmospheric scattering, such as dust, and underocculting from guiding errors may cause rapid brightenings and brightness fluctuations in the filtergrams. Difficulties in interpretation arise from superposition of different regions in the optically thin corona. In this study the procedures were relatively subjective, although basically similar to those used in solar observations of H-alpha flare brightness. These are bracketed into faint (F), normal (N), and bright (B) categories based on "naked eye" observations. Here, the coronal brightness is divided into five categories: very dim (too faint for any observed detail or structure); dim (basic form but very thin optically); moderate (average brightness of most regions); bright (brighter than normal with very visible spots or areas); and very bright (extremely visible area). Since the film contrast was inconsistent, an attempt was made to evaluate region brightness relative to the solar limb brightness. Films with extremely poor contrast were not considered. λ5303 photographs are not well-suited for intensity

studies; a better method is to obtain calibrated intensities for Fe XIV, which are listed in the Quarterly Bulletin of Solar Activity of the IAU.

Increased definition of a coronal region may be an indication of the strength of the magnetic flux within the loops. How clearly resolved the coronal loop appears could be related to higher density material concentrated in the flux tube and held in place by the stronger fields. Highly defined coronal loops which are less diffuse may also be indicative of current-producing non-potential fields, resulting in azimuthal fields pinching and confining the material. According to Parker (1977), if the azimuthal field becomes 3.97 times stronger than the longitudinal field, the loop buckles and reconnections and field annihilations could occur. The categories used in determining the definition were less subjective than those used for bright ness: (1) no resolution of features; (2) resolution of one or two loops or features in a region; (3) resolution of several loops or other features, such as "hairpins" and/or "bridge-like" structure; and (4) clear resolution of most of the region into structural features, arcades, and loop systems.

An examination was attempted of the green line corona filtergrams for open or closed fields and their relationship to H-alpha flares to see if any of the

the several flare theories concerning magnetic configuration could be supported. These various flare models are reviewed in a paper by Priest (1976).

The angular extent and percent coverage of brightness within the regions were chosen as parameters since they should be related to the area size of the corresponding chromospheric active regions. This was simply a measure in degrees of the latitudinal extent of the coronal region and the percentage of brightness along the base to the total angular lengths of the region.

The magnetic complexities of the coronal regions were inferred from the appearance of the magnetic loops and arches in λ5303 and their correlations with the Mount Wilson Magnetograms. Since there is a temporal lag between the observation of the coronal regions on the limb and the observations of the magnetograms on the disk, it was assumed that the magnetic configuration would not change appreciably over several days. The regions were divided into four classes: coronal region too weak or diffuse to resolve into features and the magnetograms showing weak diffuse fields (0); simple, bipolar (1); multipolar with some appearance of stress in the region (2); and complex, in which the region appeared too complex to resolve into features (3).

The parameters were correlated with an H-alpha flare index and a Sudden Ionospheric Disturbance (SID)

index. There seems to be little correlation between the importance and size of an individual H-alpha flare and the occurrence of a SID in the earth's atmosphere; a sub-flare may produce a SID occurrence and a larger, more important flare may not. This has been a mystery, and one wonders if the height of the green-line corona might be related to the amount of x-ray producing SID's relative to the amount of H-alpha flares produced. In a previous study by Rust and Webb (1976) of soft x-ray observations of large-scale coronal active region brightenings, it was discovered that only forty-four percent of the x-ray events were correlated with reported H-alpha flares. Also in the study by DeMastus, et al. (1973) of coronal disturbances, H-alpha flares inconsistenly produced green-line transients. A SID index and an H-alpha flare index were devised so that their ratios could be plotted against heights of the regions. The H-alpha index was measured by multiplying a weighting factor for reported brightness times the reported flare area. Flares reported with the same flare areas, but with different H-alpha intensities; i.e., faint, normal, or bright do not have equal energies and should not be treated as the same quantities in a flare index. In the present study, faint flares were weighted as 1.0, normal flares as 1.5, and bright flares as 2.0. This is somewhat arbitrary, but with equal areas this method

gives bright flares twice the value of faint flares. Only those flares which were confirmed and reported in the Comprehensive Reports were used. All flare events reported for the region from the limb to the CMP were then summed. This summation should represent the flare activity that occurred in a particular region for the first half of the visible disk passage. Because the region may change in character and strength as it moves across the disk, the period from CMP to west limb passage was not considered. Some of the regions included still developed rapidly enough to produce a small flare index with no visible λ5303 corona during the time of its limb passage--this, however, was rare.

SID's are reported in the Prompt Reports by region number, importance, and type. The SID index was compiled by weighing the importance of the SID and multiplying by the wide-spread index which is reported in the Prompt Reports. The index was then summed for all the events in a region from the limb to the CMP. The ratio of the SID index to the H-alpha flare index was evaluated by two different methods: one method was to measure the ratio of individual SID index to the index of their associated flares, summing and then evaluating the mean; the other method was to evaluate the ratio of the total SID index to the total flare index for that region.

3.4 Results

The various parameters are tabulated in Tables 3 and 4. For the year, there were 75 days of useable coronal observations, 3 days not considered because of very poor film contrast, and 288 days of observations that were not available. Out of the 75 days, 53 cases were observed with extremely faint or no λ5303 corona. A comparison with H-alpha data showed that 94% of these days of very low or no coronal activity had very insignificant or no associated chromospheric regions, and no flare or flare-related events between the east limb and the CMP. Six percent of the cases had no visible green-line corona; however, flares did occur. These cases were apparently from rapidly developing regions. There were no reported calcium plage areas within 25 or more degrees of the limb and the flares occurred after development of the calcium plage. There were 26 days of observed λ5303 coronal regions on the limb. Of these 26, 61% had reported, confirmed flares in the regions between the east limb and the CMP. If only those with definitions greater than one were considered, there were twenty days observed with green-line emissions with 75% confirmed flares reported.

There were only 18% flares reported from all regions categoriezed as definition 1 (11 cases total); these has a mean flare index of 1.03 square degrees

TABLE 3

λ5303 CORONAL REGIONS OF THE EAST LIMB FOR 1973

Date	McMath Region	Height (km)	Brightness	Definition	Angular Extent°	% Angular Extent	Complexity	Flare Index	SID Index
11 JAN	180	50,000	2	2	15	93	1	0	0
	186	106,000	3	2	12	75	1	1.9	0
	181	60,000	2	1	5	?	?	0	0
16 JAN	188	60,000	2	3	3	60	1	0	0
	193	50,000	3	2	10	60	2	0	0
23 JAN	203	50,000	2	1	8	63	1	0	0
24 JAN	205	87,000	4	4	13	54	2	5.6	0
02 FEB	218	87,000	2	1	13	69	0	0	0
05 FEB	217	69,000	3	3	8	63	1	0.7	0.5
16 MAR	275	0	0	0	0	0	0	0	0
	276	0	0	0	0	0	0	0	0
	277	0	0	0	0	0	0	0	0
19 MAR	278	0	0	0	0	0	0	0	0
12 APR	315	?	1	1	10	?	?	0	0
17 APR	322	125,000	2	3	10	60	2	22.5	1.9
07 MAY	341	0	0	0	0	0	0	0	0
08 MAY	348	0	0	0	0	0	0	0	0

TABLE 3, CONTINUED

Date	McMath Region	Height (km)	Brightness	Definition	Angular Extent°	% Angular Extent	Complexity	Flare Index	SID Index
10 MAY	349	0	0	0	0	0	0	1.0	0.5
02 JUN	375	0	0	0	0	0	0	1.2	0
03 JUN	376	0	0	0	0	0	0	0	0
04 JUN	377	50,000	3	1	10	?	0	0.9	0
14 JUN	394	87,000	3	1	11	60	0	0	0
18 JUN	398	69,000	4	4	6	40	1	5.6	1.0
	403	65,000	1	1	8	?	0	0	0
	402	59,000	3	4	8	50	1	3.5	0
11 JUL	440	0	0	0	0	0	0	0	0
30 JUL	474	0	0	0	0	0	0	3.4	0.5
03 AUG	475	0	0	0	0	0	0	0	0
11 AUG	480	0	0	0	0	0	0	0	0
17 AUG	488	?	1	2	6	?	1	0.4	0
22 AUG	497	69,000	3	2	5	90	1	3.1	0
	503	0	0	0	0	0	0	3.1	0
	500	50,000	2	2	6	30	1	0	0
23 AUG	501	50,000	3	3	12	60	1	0	0
25 AUG	504	low	?	1	12	?	?	0	0

TABLE 3, CONTINUED

Date	McMath Region	Height (km)	Brightness	Definition	Angular Extent°	% Angular Extent	Complexity	Flare Index	SID Index
27 AUG	508	0	0	0	0	0	0	0	0
12 SEP	524	60,000	1	1	5	?	?	0	0
	522	78,000	3	3	12	70	1	2.0	0
21 SEP	0	0	0	0	0	0	0	0	0
23 SEP	539	0	0	0	0	0	0	0	0
24 SEP	540	60,000	5	2	6	50	3	6.8	1.0
	537	41,000	1	1	12	?	0	1.2	0
	541	41,000	1	1	3	?	0	0	0
25 SEP	542	115,000	5	4	13	69	1	9.3	0.5
26 SEP	543	87,000	1	2	12	60	3	6.8	0
27 SEP	545	87,000	3	3	18	80	2	0	0
16 OCT	577	60,000	3	3	17	65	2	0	0
19 OCT	583	0	0	0	0	0	0	0	0
23 OCT	588	69,000	3	3	4	75	?	2.3	0
	589	69,000	2	2	4	50	1	0.4	7.5
	590	69,000	2	2	10	60	1	15.0	0.5
	584	87,000	3	3	8	75	3	19.0	0.5

TABLE 3, CONTINUED

Date	McMath Region	Height (km)	Brightness	Definition	Angular Extent°	% Angular Extent	Complexity	Flare Index	SID Index
24 OCT	592	LOW FILM CONTRAST							
	590	LOW FILM CONTRAST							
12 NOV	618	69,000	2	3	7	50	2	7.7	0
11 DEC	657	0	0	0	0	0	0	0	0
20 DEC	667	0	0	0	0	0	0	0	0

TABLE 4

SID PRODUCING REGIONS

Date/Time	Region	SID Index	Associated Flare Coordinate	H-Alpha Flare Index	SID IN. / H-α IN.	Height of λ 5303	Remarks
10 FEB/0857	217	0.5	N07	-F	0.7	?	(left of region) Weak, open field
21 MAR/1158	275	0.5	CANNOT FIND H-ALPHA DATA				
17 APR/2251	322	0.5	N13	1.5(0.27)	1.2	115,000	Between loops
18 APR/1417	322	5.0	N10	(0.15)	33.3	115,000	Possibly open rays
19 APR/0006	322	0.5	N11	1.5(0.65)	0.51	115,000	Possibly open rays
20 APR/1405	322	0.5	N11	(0.36)	1.4	115,000	Possibly open rays
21 APR/0650	322	1.5	N08	1.5(0.69)	1.45	115,000	Possibly along spike
21 APR/1006	322	0.5	N11	(0.19)	2.6	115,000	Possibly open config.
21 APR/1558	322	0.5(5)	N14	(0.90)1.5	1.85	78,000	
22 APR/1227	322	0.5	N13	(0.17)	2.9	115,000	Possibly along spike
22 APR/1504	322	5.0	N12	(1.26)1.5	2.6		Possibly open
22 APR/1820	322	0.5	N13	1.3(0.39)	0.85	115,000	Possibly along spike
22 APR/2146	322	5.0	N13	1.5(1.7)	1.96	115,000	Possibly along spike
23 APR/1703	322	0.5	N11	(0.80)	0.6	97,000	Possibly along spike
20 JUN/0900	398	0.5	S03	0.38	1.3	60,000	Between loops
24 JUN/0218	398	0.5	CANNOT FIND H-ALPHA DATA				

TABLE 4, CONTINUED

Date/Time	Region	SID Index	Associated Flare Coordinate	H-Alpha Flare Index	SID In. / H-α In.	Height of λ 5303	Remarks
05 AUG/2336	474	0.5	N06	(1.19)1.5	0.28	-	
28 SEP/0746	540	0.5	S14	0.41	1.2	87,000	Edge of region
01 OCT/1803	540	0.5	S14	(0.51)1.5	0.65	87,000	Edge of region
30 SEP/1421	542	0.5	S13	0.50	1	106,000	Possibly open
27 OCT/1547	590	5(1.5)	N18	3.74 (2)	0.2	69,000	Edge of loop
26 OCT/2240	584	0.5	S16	0.62(1.5)	0.54	87,000	

(modified by the brightness weighting). Regions of definition 2 (13 cases) had 61.5% flares with a mean flare index of 3.17 square degrees. 60% of those regions observed as definition 3 (10 cases) had flares before CMP and a mean flare index of 9.3 square degrees. 100% of those regions observed as definition 4 flared; however, there were only four observed cases. The flare mean was 6.02 square degrees for regions of definition four. There appears to be a definite correlation between flare activity and the resolution of the coronal loops (Figure 16).

There was some evidence of a correlation between green-line coronal heights and their associated flare indexes. The correlation coefficient for this was 0.67 with 16 cases. This correlation suggests that the height of the λ5303 corona could be indicative of the amount of flare activity that may be expected. However, higher coronal regions do not necessarily guarantee flare occurrence. Combining this result with that of coronal regions having definitions greater than 1 may lead one to expect a 75% chance of flare occurrence between the east limb and the CMP with the greater coronal heights suggesting greater activity. The height vs. flare index plot shows wide scatter and the statistical base is very small. More observations should be taken to make this correlation more definitive. There

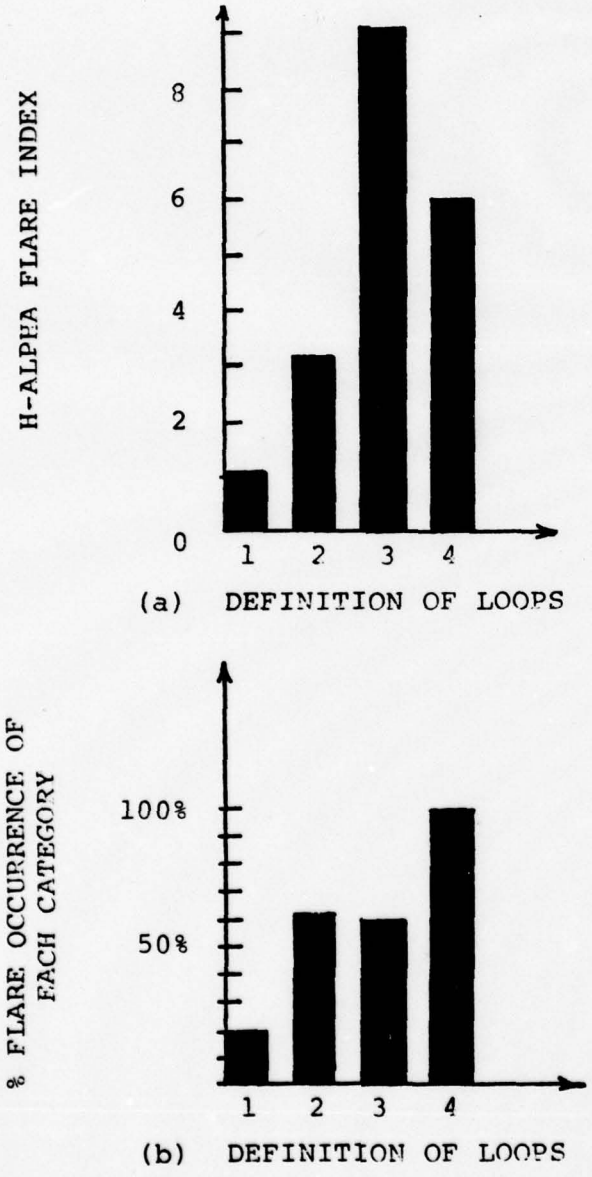

FIGURE 16. λ5303 loop definition histograms for 1973. Definitions: (1) no structure identifiable; (2) one or two loops resolved; (3) several loops or other features, such as "hairpin" or "bridge-like" structures identifiable; (4) clear resolution of most of regions into features; arcades and loop systems clearly identifiable.

are gaps in the H-alpha reported data as well, which may account for some of the statistical scatter (Figure 17).

There is no apparent relationship between brightness, angular extent, or complexity as defined here, and flare activity. The method used to evaluate brightness was somewhat subjective and, therefore, may not be an accurate measurement of correlation; however, in some cases within the same film frames fainter regions out-produced the brighter regions in flare activity. Based on this, there seemed to be a real lack of correlation between brightness of the green-line corona and the chromospheric flares. DeMastus, Wagner, and Robinson (1973) seemingly found the same result in their study of green-line coronal transients: the detectability of λ5303 transients was not particularly dependent on coronal intensities. A likely explanation of this was that the emission of Fe XIV may give way to that of the more highly stripped ions of iron over the hotter regions. As the emission of Fe XIV increases, the emission of λ5303 may then decrease as the Fe XIV ions become more scarce. Based on this, yellow-line calcium may be more informative than the extremely hot areas. It was surprising that the magnetic complexity of the region as viewed in λ5303 did not correlate highly with the occurrence of

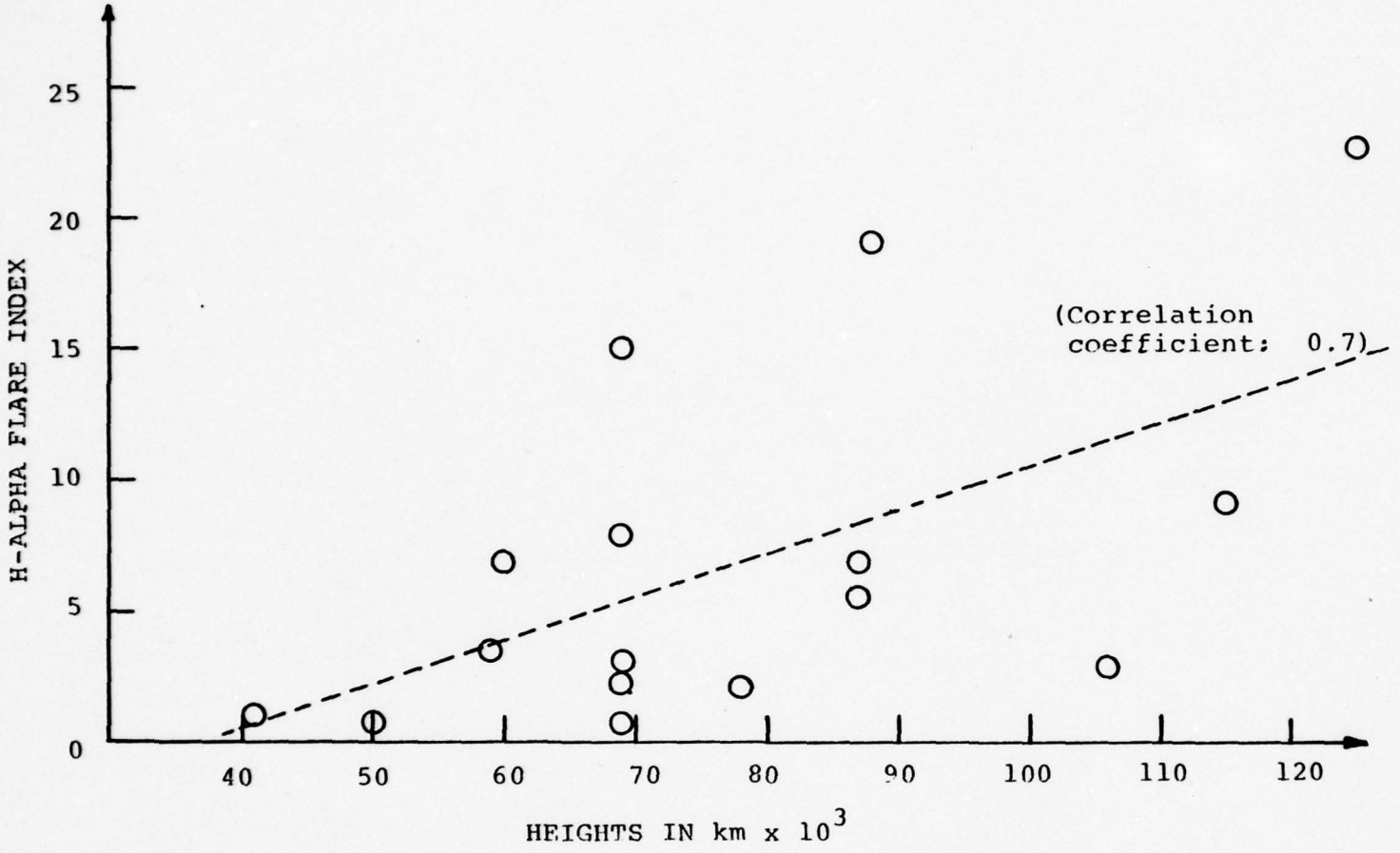

FIGURE 17. Coronal region height vs. H-alpha flare index for 1973.

flares within the region. There were 10 out of 15 cases (66%) where flares were produced in those regions designated 1. 3 out of 6 cases (50%) had flares for category 2, and 3 out of 3 (100%) for category 3. This indicated that a region categorized as 2 had a 50% chance of producing or not producing flares. The mean flare index was 4.2 square degrees (modified by the brightness weighting), 11.9 square degrees, and 10.9 square degrees respectively for the three categories. It appears that if regions are flare-producing, the more magnetically complex coronal regions have higher flare indexes and are more active as one might expect. More observations are needed for meaningful statistics.

There was no apparent correlation between SID's and any observable green-line coronal structure; and no relation was found for the ratio of SID's to H-alpha flare occurrence and coronal heights. Also, no supporting evidence was found for the idea of two different classes of flares as discussed by Rust. As a measure of the energy density of flares, the mean ratio of the flare importance to flare area of each region was found. This was correlated with λ5303 coronal heights to see if there was an anti-correlation; i.e., the high energy density flares occurring low in the solar atmosphere versus larger area, lower energy density flares occurring higher in the corona. There was no correlation.

Spatial correlation with the green-line corona and H-alpha flares showed that frequently the locations of the flares were between coronal loops or at the boundaries of visible coronal regions. In a few cases the flares occurred in areas of faint corona and magnetic structures were difficult to infer. Several flares occurred in areas of open magnetic fields. There were 24 reported cases of confirmed flares and sub-flares between E75 and E90, and within one day of the limb passage of the coronal regions studied. Eighteen of the flares appeared to be located along the edges of the loop systems; there were no clearly evident cases where the flares were observed directly under coronal loops. In some cases, higher diffuse arches could be seen over the flare locations.

3.5 Specific Regions

In a distinctive coronal region observed on 24 January, a brilliant sub-flare occurred between two pronounced loop systems. The flare occurred on 25 January along with a spray at the base of the loop system at the northern edge of the coronal region. The two loop systems appeared oriented at angles to each other with the southern loops having a "hairpin" appearance and the northern loops appearing more "bridge-like." Another flare was reported in a weaker,

fainter area to the south of the coronal region with an apparent arch over the flare location. Mount Wilson Magnetograms on 27 January showed the intrusion of a negative magnetic region between two positive areas. The fields appeared to be sheared such that currents might flow in the coronal loops. The region was identified with McMath region 205. The flare index was 5.58 from the limb to the CMP for this region. The coronal loops were about 87,000 km high with a bright, highly defined loop structure. Superposition of the coronal region and the Fraunhofer map showed some quiescent prominences in the quiet corona on both sides of the region. There is no apparent association with these and Fe XIV emission (Figure 18).

Another interesting region occurred in 17 April. This region featured high, faint loops and arches that extended over 10° latitude. The visible corona, although not bright, reached 125,000 km. This coronal emission was associated with McMath 322 and produced 28 flares on the visible disk. The flare index was 22.45 square degrees (modified by brightness weighting). The associated H-alpha flares were again located between the coronal loops (Figure 19). On the 18th, a bright surge was reported along the boundary of one loop and an eruptive prominence occurred. The prominence was under a system of loops whose longitudinal fields were

24 JAN 1973 - λ5303 Corona

18 JUN 1973 - λ5303 Corona

Enhanced View of 24 JAN 1973

Enhanced View of 18 JUN 1973

PHOTO SCALES ARE SMALLER THAN MAGNETOGRAMS BY 15.5 cm: 17 cm DISK

28 JAN 1978

Mt. Wilson Magnetogram (Intepreted Loop Structure)

20 JUN 1973

Mt. Wilson Magnetogram (Interpreted λ5303) Photo Smaller Scale, 15.5 to 17 cm

FIGURE 18. λ5303 corona and magnetograms for 24 January 1973 and 18 June 1973.

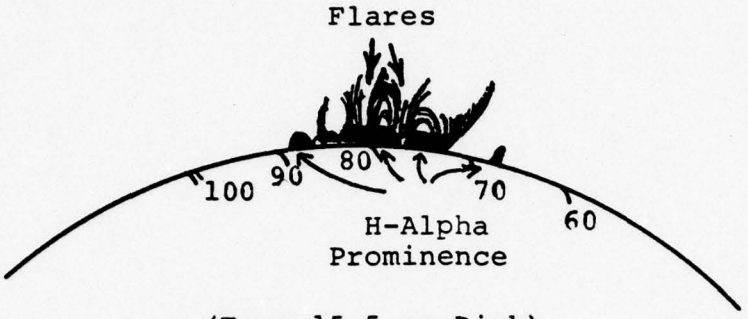

(From 15.5 cm Disk)

19 April, Mt. Wilson
Magnetogram
(Inferred Magnetic Fields)
(Scale: 17 cm Stoneyhurst)

FIGURE 19. 17 April 1973 λ5303 coronal region.

apparently transverse to the length of the prominence. This could be seen as green-line emission apparently looping over the prominence, verified by the Mount Wilson magnetograms showing east-west oriented magnetic fields. The magnetograms again suggested that there might be shearing between the loops. The faintness of the solar limb and coronal features indicate that the film contrast may have been very low.

The coronal region of 18 June looked like the typical low-lying, well-resolved, flare-associated loops which Dunn (1971) observed. However, at this time there were apparently none of the H-alpha flare loops present. Flares did occur between the flare-type loops that were "hairpin" shaped and the brighter "bridge-like" loop systems to the north. The magnetogram showed two bipolar regions close together with good opportunity for reconnections and apparent shear between loops. The flare indexes were 5.64 and 3.5, respectively, for the associated McMath regions 398 and 402 (Figure 20).

Two other noteworthy coronal regions occurred on 25 September and 23 October. The second region was a return of the first since their locations were the same and the intervening period was about 27 days. Also, their character and appearance were very similar. On 25 September the height of the corona was 115,000 km and the associated flare index was 9.34. On 23 October

λ5303 - 25 SEP 1973

λ5303 - 23 OCT 1973

Enhanced View of 25 SEP 1973

Enhanced view of 23 OCT 1973

(a) 26 SEP 1973 Magnetogram With Inferred Loops (Scale Photo to Magnetogram, 15.5:17 cm)

(b) 25 OCT 1973 Magnetogram (Scale Phototo Magnetogram, 15.5 cm to 17 cm Disk)

FIGURE 20. λ5303 corona and magnetograms for (a) 25 September 1973, and (b) 23 October 1973.

the height was about 87,000 km and the flare index was 19 square degrees (modified by brightness weighting). The region appeared brighter on 25 September than on 23 October, but this may have been a difference in film contrast. On 23 October the flares were again apparently located along the edges of the visible coronal loops (Figure 20).

In summary, analysis of the filtergrams show that the resolutions and heights of coronal loops observed on the limb may be correlated with chromospheric flare activity. The correlations appear weak, but there may be some physical justifications for them, as discussed in Chapters III and IV. There were no correlations found for the intensities or angular extents of these regions. It is very likely that as the iron becomes more fully ionized with higher temperatures the density and, therefore, emission of Fe XIV decreases. Also, no correlations were found for sudden ionospheric disturbances, which are flare produced, with any of the features of the λ5303 corona examined. The relationship between SID occurrences and flare size and intensity would be a worthwhile study.

Specific regions were examined for the relationship between their structure and flares. Some of the regions that produced flares seemed to be in stressed configurations, with arcades of loops that appeared

oriented at angles relative to others. Reported flare occurrences in the chromosphere appeared to be at the footpoints of the coronal loops and sometimes appeared to occur at the visible boundaries of the coronal regions. It seems reasonable that in these stressed configurations, field-aligned currents could flow in the lower coronal loops.

The difficulties in observing and analyzing the λ5303 survey filtergrams were many and, therefore, the results could be misleading; however, the inferences drawn from these results are not out of line with current views of many scientists.

CHAPTER IV

INTERPRETATIONS

Although the data examined has been interpretive and somewhat ambiguous, it suggests a hypothesis that flare mechanisms and eruptive prominence mechanisms are basically the same. Much of the current literature suggests that flares and eruptives are not only related, but also that prominences, as Sturrock proposes, may be the storage mechanisms for flares. The quiescent prominences which erupt are generally footpointed in weaker magnetic regions and are apparently not associated with H-alpha flares, but are related to x-ray brightenings in the corona (Webb, et al.) which Rust (1977) calls "Coronal Flares." As Rust suggests, H-alpha emission would not be observed because the coronal flare may not produce enough heat or accelerate enough particles into the chromosphere. The typical pattern that emerges is that shear in photospheric magnetic fields may induce field-aligned currents into the footpoints of the prominences. The shear may be produced by sunspot rotation, lateral motions, or photospheric differential rotation. The currents would

be transmitted along the flux strands of the prominence into the lower corona and store energy via increasing azimuthal fields around the prominence. The energy release may come after the aximuthal fields become sufficiently stronger than the longitudinal fields for eruptions to occur, possibly due to buckling (Parker, 1977) which may result in reconnections and annihilation of the twisted field. If numerous small reconnections occur between small filament strands and/or if ohmic dissipation lowers the rate of current increase, the prominence may remain in a quasi-stable state with no eruption (Malville, private communication). If high frequency plasma waves are moving through the plasma, then through anomalous resistivity localized Joule heating could occur in the flux tube which may lead to an eruption. If the prominence is footpointed in large magnetic fields with strong gradients, then the coronal x-ray brightening that occurs due to the eruptive may be of sufficient strength to accelerate particles along the flux tubes or filament channel back into the chromosphere where H-alpha brightenings are seen as flares. If the magnetic fields of the footpoints are weaker, then only the coronal brightenings may occur with the eruptive. That field-aligned currents may grow in all prominences is implied from the observations in Chapter II and, as discussed, may be a function of

certain filament parameters such as tilt angle-to-length ratios, area-to-length ratios (although this was not observed), and the relative velocity between the footpoints. Untwisting filaments before eruptions and before flare occurrences have been observed which also imply stressed fields and current flows (Rust, 1977). If stretching of the field lines may induce currents, then one may expect the heights of the flux tubes to increase with the widened distance between footpoints and a possible correlation with flares or eruptives. There may be a critical height involved, as observed by Thompson and Billings (1967) in their prominence studies. This could not be seen in my observations of prominences, but may be indicated by the relationship between λ5303 loop heights and flare occurrences shown in Chapter III. Since Klesek found that λ5303 loops sheathed flare-associated H-alpha loops (Dunn, 1971), it is probable that as the promi-nences rise and untwist, the λ5303 loops also rise and possibly untwist.

For flares that sometimes seem to occur with no visible H-alpha prominence, it may be that the current-carrying coronal loops are visible in other wavelengths, such as the λ5303 line. The increases in resolution that were found in association with flare occurrences noted in Chapter III may indicate that currents flow

in the coronal loops which increase the azimuthal fields around the flux tube, confining the material, thereby increasing the material's density and resulting in the higher resolution. If this were the case, one might expect to see λ5303 eruptions occurring. Transients are observed that disrupt the coronal loops, but they are generally seen to reform without much structural change within a short time (DeMastus and Wagner, 1973). This seems reasonable if no significant change occurs in the photospheric fields which are probably the driving mechanisms (Tanaka, 1976; Krieger, et al., 1976; Rust, 1976, 1977).

Observations of the coronal event of 24 January 1973 (Figure 18), noted in Chapter III, supports some of the above conclusions. The spray occurred on one side of the loop system with the sub-flare on the other side. The loop systems appeared oriented at different angles to each other and shear reconnections and field annihilation may have occurred in the low corona which accelerated particles into the chromosphere along both sides of the loop system. No H-alpha prominences were seen in the vicinity at the time of λ5303 observation. A simple calculation of particle drifts was made for the loop system on the assumption that the loops were circular and that drifts due to centrifugal force might throw the accelerated particles out of the flux tube

before reaching the footpoints in the chromosphere. A large coronal loop field of 200 Gauss (Rust, 1977) was assumed within the flux tube and 10 keV electrons. This yielded electron velocities of 1.5×10^{10} cm s^{-1} which is typical for velocities of plasmas (de Jager, 1969). The drift was computed from

$$v_d = \frac{(\hat{R}_B \times \hat{B})}{\Omega R_B} (v_{||}^2) = \frac{v_{||}^2}{\Omega R_B}$$

for circular loops and the loop radius $\hat{R}_B \perp$ to $\hat{B}$. $v_{||}$ is the velocity along the loop. $\Omega \equiv$ gyrofrequency and is given by

$$\Omega = eB/mc = 3.5 \times 10^9 \text{ rad } s^{-1}$$

then

$$v_d = \frac{(1.5 \times 10^{10} \text{ cm } s^{-1})^2}{(3.5 \times 10^9 \text{ rad } s^{-1})(7.6 \times 10^9 \text{ cm})}$$

$$= 8.5 \text{ cm } s^{-1}$$

for a loop system of 76,000 km in height. If the particles were accelerated from the top of the loops, then

$$\frac{\pi}{2} R_B \approx 1.2 \times 10^{10} \text{ cm} \quad \text{(for ¼ circumference)}$$

and the transit time for the particles would average 0.80 seconds at their velocity. The drift in that time would be less than seven centimeters. If the magnitude of the coronal field in the flux tube was considered

to be 50 Gauss, which is approximately an order of magnitude lower (Hyder, 1965; Harvey, 1968), the drift would still be less than one meter. This indicates that the accelerated particles should strike the chromosphere at the footpoints of the flux tubes which make up the coronal loops.

The measurements taken imply that field-aligned currents may flow in prominences due to shear induced by photospheric differential rotation, and in some flare-associated λ5303 loop systems as implied by the more sharply defined flux tubes. This also suggests that energy storage may be possible in prominences and in loops visible in other lines--specifically, λ5303. The ideas of Sturrock, Rust, and others who suggest that prominences may have a direct role in flare production, are very promising (Rust, 1976, 1977). Further, since the total energies released in prominence eruptives, both active and quiescent, are comparable to flare energies and may produce the type of coronal x-ray brightenings that are flare related, the "disparition brusques" may be the primary energy release phenomena and the H-alpha flares secondary. Strong support of this idea is given by Roy and Tang (1975) who observed that pre-flare filament activation is accompanied by slight x-ray enhancement, and that x-ray emission is synchronized to phases in filament

activations with rapid increases in soft x-ray flux accompanying the fastest filament expansions; and plateaus and slow decay phase in x-rays are associated with slowing and termination of filament expansion. Rust concludes, based on observations of Martin and Ramsey (1972), that a majority of flares are preceded by filament activation.

As previously mentioned, observations also indicate that emerging flux regions and overlying coronal fields may affect the storage of energy in the flux tubes, with emerging flux regions causing reconnections resulting in the release of the stored energy. Higher coronal magnetic fields may increase the stability and increase the energy storage because of higher magnetic pressure pressing down on the prominences or low coronal loops. Changes in these overburdening fields may then cause eruptions.

CHAPTER V

FLARE PREDICTION

One of the most important and useful aspects of solar flare studies is that of flare predictions and prediction parameters. The λ5303 corona apparently contains some of these parameters for medium and long-range predictions (approximately one to seven days). One can predict with fair probability that flares will occur in a region within the next seven days by the presence of the Fe XIV coronal region on the east limb, along with the appearance of any structural features. The height of the region and the resolution of its features suggests the amount and intensity of the forecasted flare occurrences. Higher resolution λ5303 filtergrams on the order of 3/4 to 1 Å bandpass are needed to give better observations of magnetic structure and to provide better guidance in forcasting flare locations. Daily, or more often, high resolution filtergrams would allow studies of slow-motion movements of the quasi-stable coronal features which may precede flare events and provide important flare predictors. These types of studies should be invaluable for understanding flare physics and flare morphology.

Correspondence between high resolution coronographs and high resolution magnetograms should allow three-dimensional images of coronal structures formed entirely from ground-based equipment. Position of real-time H-alpha filtergrams under the λ5303 corona should provide precise spatial and temporal associations between chromospheric and coronal structure and events. It is hoped that the new λ5303 coronagraph that is currently being completed at Sacramento Peak Observatory will have some or all of these features and prove to be a valuable source of information for flare physics studies and flare predictions (R. Smart, private communication).

As the characteristics and changes in morphology of prominences and their association with flares becomes better understood, they could provide important short-range (less than one day) flare predictors. For example, rapid changes in the tilt angle-to-length ratios in active filaments may indicate an impending flare, and increases in prominence heights with any apparent twisting or untwisting may forewarn a flare. If an idea of the magnetic field strengths and current flows or rates of change of currents in prominences could be determined quickly, it is possible that the time required to buckle could be easily determined and used as a flare prediction parameter.

REFERENCES

Bohlin, J. D., 1977, Coronal Holes and High Speed Wind Streams, (Colorado Association University Press, Boulder; J. B. Ziiker, ed.), p. 31-35.

De Jager, C., 1969, Solar Flares and Space Research (Reidel Publishing Co., Amsterdam; C. De Jager and Z. Svestka, eds.), p. 2-9.

DeMastus, H., 1977, "Sunspot Motions and Flares," paper presented at the SOON Data Collection and Archival Conference, 26 April.

DeMastus, H. L., Wagner, W. I., and Robinson, R. D., 1973, Solar Phys. 31, 449-459.

Dolder, F. P., Roberts, W. O., and Billings, D. E., 1954, Astrophys. J. 119, 120-124.

Dunn, R. B., 1971, Physics of the Solar Corona (Reidel Publishing Co., Dordrecht-Holland; C. J. Macris, ed.), p. 114-129.

Engvold, O., Malville, J. M., and Rustad, B. M., 1976, Solar Phys. 48, 137-148.

Frankenthal, S., 1976, "Dilation of Force-Free Magnetic Flux Tubes," American Science and Engineering, Inc., Report No. ASE-4002.

Harvey, J., 1968, Astron. J. 73, 62.

Heyvaerts, J., and Priest, E. R., 1976a, Solar Phys. 47, 223.

Heyvaerts, J., Priest, E. R., and Rust, D. M., 1976b, American Science and Engineering, Inc., Report No. ASE-4025.

Hyder, C. L., 1965, Astrophys. J. 141, 1374.

Jacobs, V. L., 1977, Astrophys. J. 211, 605.

Jockers, I., and Engvold, O., 1975, Solar Phys. 44, 429-433.

Kippenhahn, R., and Schluter, A., 1957, Zs. f. Ap. 43, 36.

Krieger, A. S., de Feiter, L. D., Vaiana, G. S., 1976, Solar Phys. 47, 118-126.

Martin, S. F., and Ramsey, H. E., 1972, in Solar Activity Observations and Predictions (MIT Press, Cambridge; P. W. McIntosh and M. Dryer, eds.), p. 371.

McIntosh, P. S., Krieger, A. S., Nolte, J. T., and Vaiana, G., 1976, "Association of X-Ray Arches with Chromospheric Neutral Lines," American Science and Engineering, Inc., Report No. ASE-3866.

Pallavicini, R., Serio, S., and Vaiana, G. S., 1977, Astrophys. J. 216, 108-122.

Papadopoulous, K., 1976, "A Review of Anomalous Resistivity for the Ionosphere," NRL Memorandum.

Parker, E. N., 1977, Annual Review of Astronomy and Astrophysics, Vol. 15 (Annual Reviews, Inc., Palo Alto, California), p. 45-68.

Petrasso, R. D., and Krieger, A. S., 1976, "The Location of the Site of Energy Release in a Solar X-Ray Subflare," American Science and Engineering, Inc., Report No. ASE-3684.

Priest, E. R., 1976, Solar Physics 47, 22.

Rust, D. M., 1973, "Solar Flares," American Science and Engineering, Inc., Report No. ASE-4218.

Rust, D. M., and Webb, D. F., 1976, "Soft X-Ray Observation of Large-Scale Coronal Active Region Brightenings," American Science and Engineering, Inc., Report No. ASE-4094.

Serio, S., and Vaiana, G. S., 1978, "Configuration and Gradual Dynamics of Prominence-Related X-Ray Coronal Cavities," Center for Astrophysics preprint Series No. 935.

Spicer, D. S., 1976, "An Unstable Arch Model of a Solar Flare," NRL Report No. 8036.

Sturrock, P. A., 1967, "Solar Flares," in Plasma Astrophysics (Academic Press, New York; P. A. Sturrock, ed.), p. 168-184.

Tanaka, K., 1976, Solar Phys. 47, 247-259.

Thompson, W. I., III, and Billings, D. E., 1967, Astrophys. J. 149, 269-273.

Webb, D. F., Krieger, A. S., and Rust, D. M., 1976, "Coronal X-Ray Enhancements Associated with H-Alpha Filament Disappearances," American Science and Engineering, Inc., Report No. ASE-3868.

Zirin, H., and Tanaka, K., 1973, Solar Phys. 32, 173.